

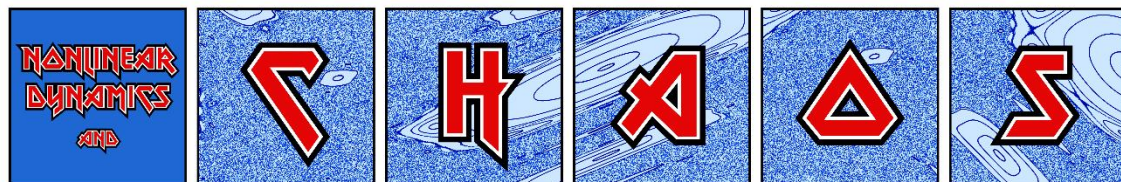
Numerical methods of chaos detection

Haris Skokos

Nonlinear Dynamics and Chaos (NDC) group
Department of Mathematics and Applied Mathematics
University of Cape Town
Cape Town, South Africa

E-mail: haris.skokos@uct.ac.za – haris.skokos@gmail.com
URL: http://math_research.uct.ac.za/~hskokos/

31st Summer School – Conference on Dynamic Systems and Complexity
10 July 2025, University of Thessaly, Lamia, Greece



Outline

- **Dynamical Systems**
 - ✓ **Hamiltonian models – Variational equations**
 - ✓ **Symplectic maps – Tangent map**
- **Brief presentation of chaos detection methods**
- **Chaos Indicators**
 - ✓ **Lyapunov exponents**
 - ✓ **Smaller ALignment Index – SALI**
 - **Definition**
 - **Behavior for chaotic and regular motion**
 - **Applications**
 - ✓ **Generalized ALignment Index – GALI**
 - **Definition - Relation to SALI**
 - **Behavior for chaotic and regular motion**
 - **Application to time-dependent and dissipative models**
- **Chaos diagnostics based on Lagrangian descriptors (LDs)**
- **Summary**

Autonomous Hamiltonian systems

Consider an **N degree of freedom** autonomous Hamiltonian system having a Hamiltonian function of the form:

$$H(\overbrace{q_1, q_2, \dots, q_N}^{\text{positions}}, \overbrace{p_1, p_2, \dots, p_N}^{\text{momenta}})$$

The time evolution of an orbit (trajectory) with initial condition

$$P(0) = (q_1(0), q_2(0), \dots, q_N(0), p_1(0), p_2(0), \dots, p_N(0))$$

is governed by the **Hamilton's equations of motion**

$$\frac{dp_i}{dt} = -\frac{\partial H}{\partial q_i}, \quad \frac{dq_i}{dt} = \frac{\partial H}{\partial p_i}$$

Variational Equations

We use the notation $\mathbf{x} = (q_1, q_2, \dots, q_N, p_1, p_2, \dots, p_N)^T$. The **deviation vector** from a given orbit is denoted by

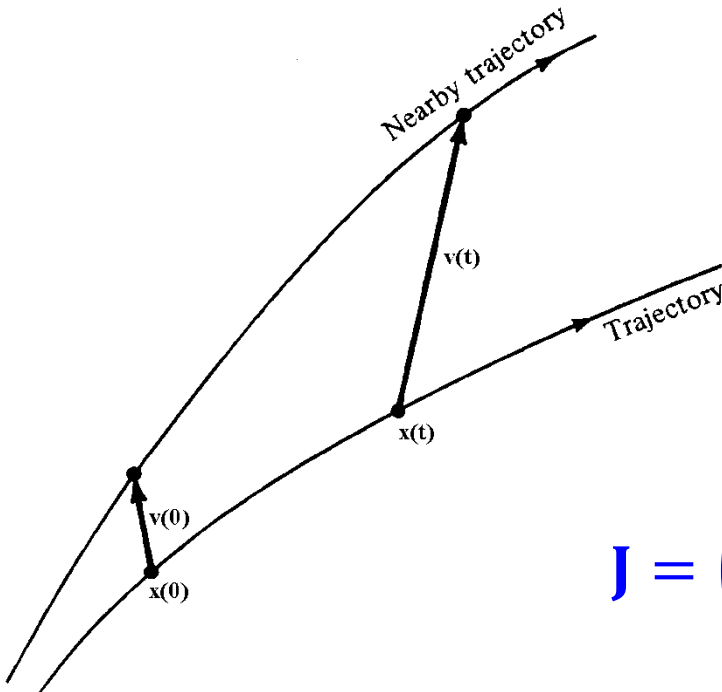
$$\mathbf{v} = (\delta x_1, \delta x_2, \dots, \delta x_n)^T, \text{ with } n=2N$$

The time evolution of \mathbf{v} is given by the so-called **variational equations**:

$$\frac{d\mathbf{v}}{dt} = -\mathbf{J} \cdot \mathbf{P} \cdot \mathbf{v}$$

where

$$\mathbf{J} = \begin{pmatrix} \mathbf{0}_N & -\mathbf{I}_N \\ \mathbf{I}_N & \mathbf{0}_N \end{pmatrix}, \mathbf{P}_{ij} = \frac{\partial^2 H}{\partial x_i \partial x_j} \quad i, j = 1, 2, \dots, n$$



Symplectic Maps

Consider an **2N-dimensional symplectic map T**. In this case we have **discrete time**.

The evolution of an **orbit** with initial condition

$$P(0)=(x_1(0), x_2(0), \dots, x_{2N}(0))$$

is governed by the **equations of map T**

$$P(i+1)=T P(i) \text{ , } i=0,1,2,\dots$$

The evolution of an initial **deviation vector**

$$v(0) = (\delta x_1(0), \delta x_2(0), \dots, \delta x_{2N}(0))$$

is given by the corresponding **tangent map**

$$v(i + 1) = \left. \frac{\partial T}{\partial P} \right|_i \cdot v(i) \text{ , } i = 0, 1, 2, \dots$$

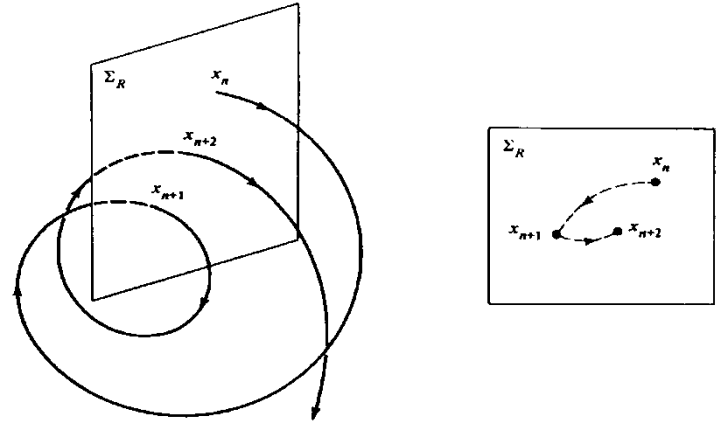
Chaos detection techniques

- **Based on the visualization of orbits**
 - ✓ **Poincaré Surface of Section (PSS)**
 - ✓ **the color and rotation (CR) method**
 - ✓ **the 3D phase space slices (3PSS) technique**

Poincaré Surface of Section (PSS)

We can constrain the study of an $N+1$ degree of freedom Hamiltonian system to a **$2N$ -dimensional subspace of the general phase space.**

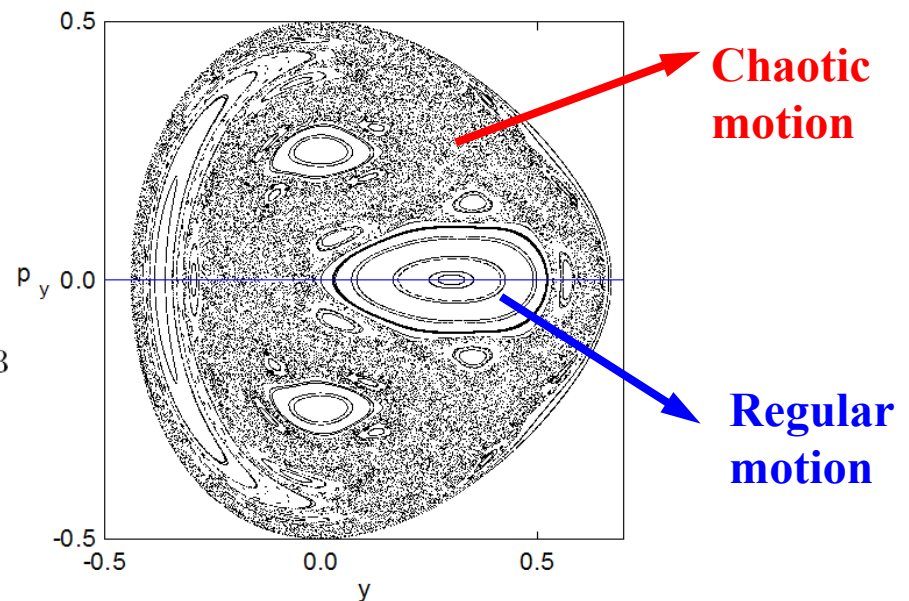
In this sense **an $N+1$ degree of freedom Hamiltonian system corresponds to a $2N$ -dimensional symplectic map.**



Lieberman & Lichtenberg, 1992, *Regular and Chaotic Dynamics*, Springer.

The 2D Hénon-Heiles system:

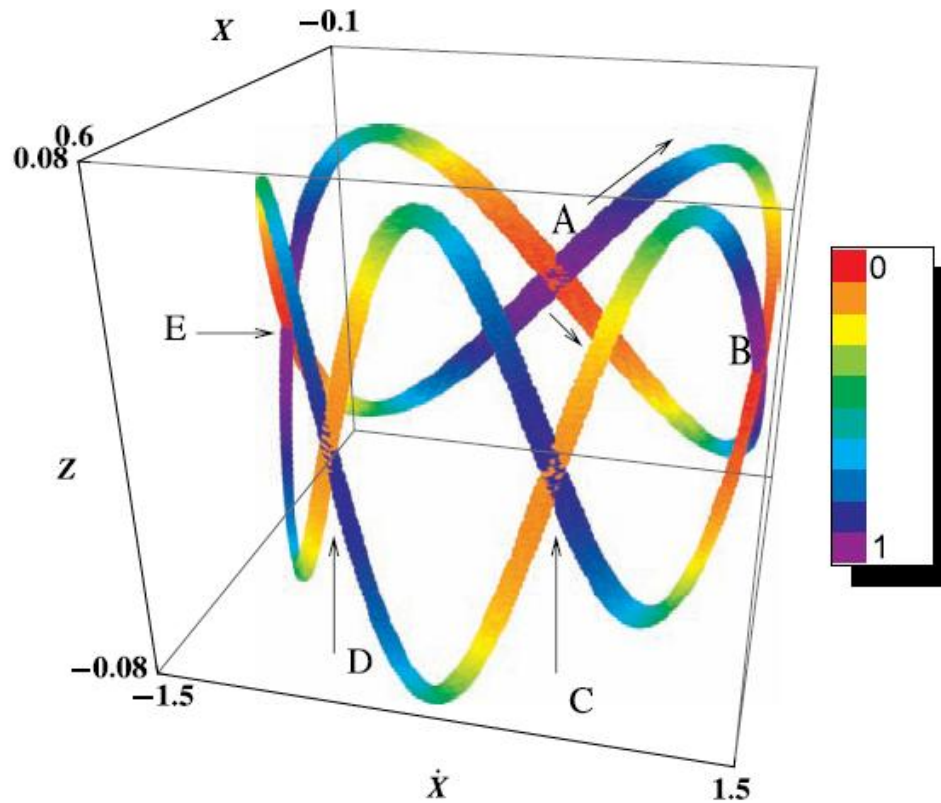
$$H_2 = \frac{1}{2}(p_x^2 + p_y^2) + \frac{1}{2}(x^2 + y^2) + x^2y - \frac{1}{3}y^3$$



The color and rotation (CR) method

For 3 degree of freedom Hamiltonian systems and 4 dimensional symplectic maps:

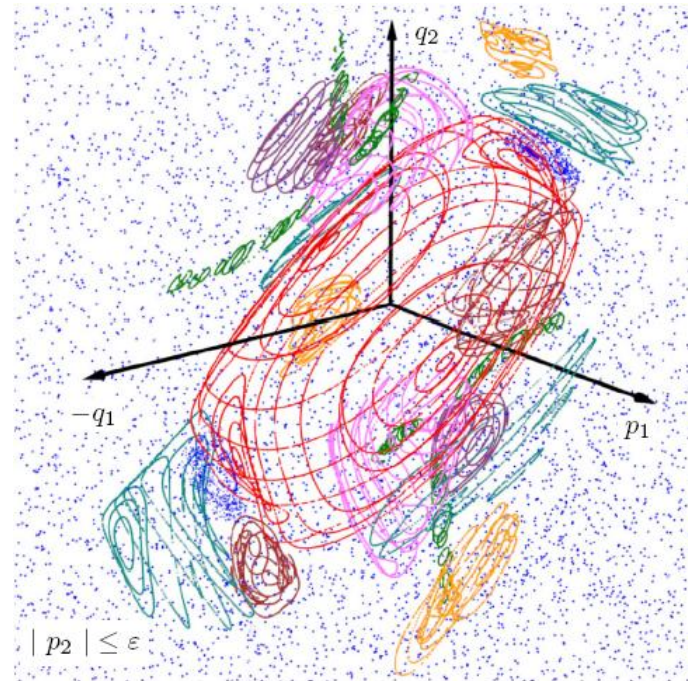
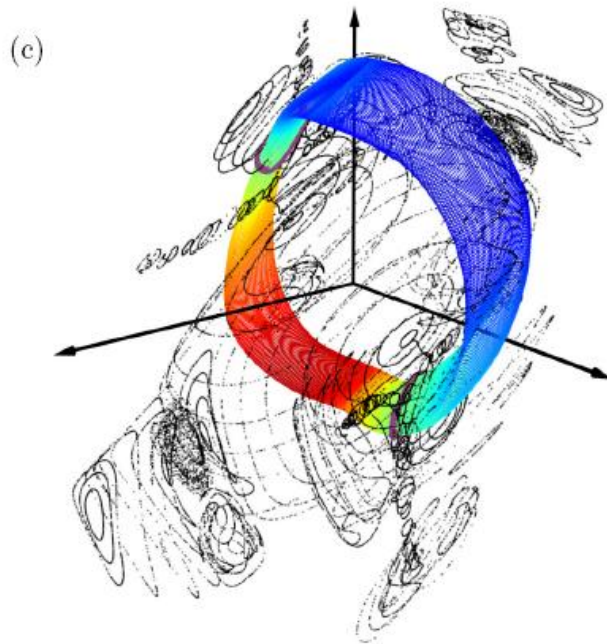
We consider the 3D projection of the PSS and use color to indicate the 4th dimension.



The 3D phase space slices (3PSS) technique

For 3 degree of freedom Hamiltonian systems and 4 dimensional symplectic maps:

We consider thin 3D phase space slices of the 4D phase space (e.g. $|p_2| \leq \varepsilon$) and present intersections of orbits with these slices.



Chaos detection techniques

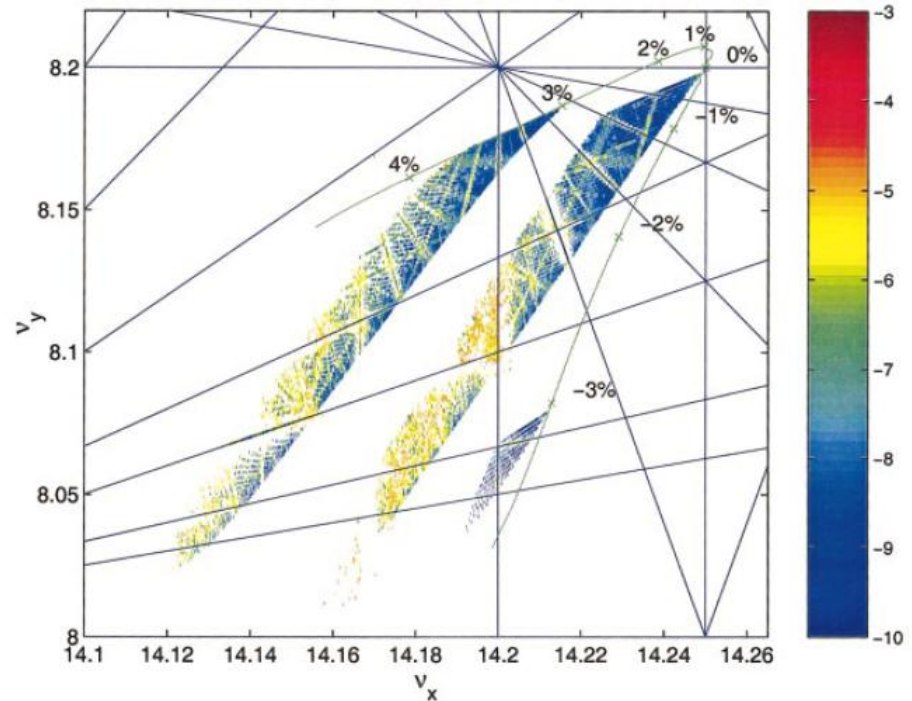
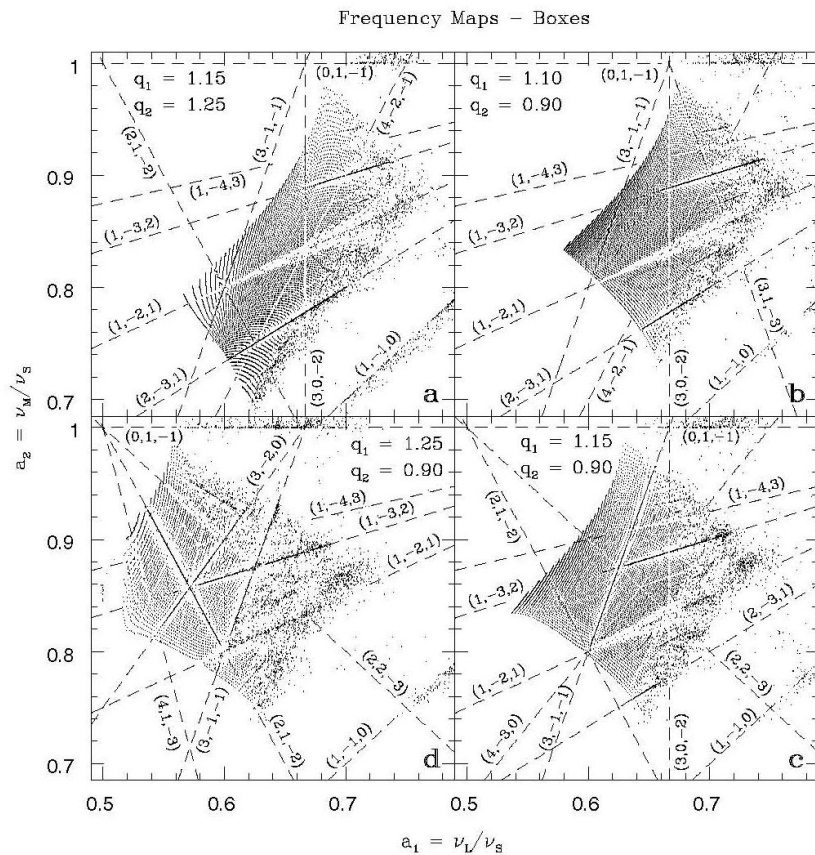
- **Based on the visualization of orbits**
 - ✓ Poincaré Surface of Section (PSS)
 - ✓ the color and rotation (CR) method
 - ✓ the 3D phase space slices (3PSS) technique
- **Based on the numerical analysis of orbits**
 - ✓ Frequency Map Analysis
 - ✓ 0-1 test

Frequency Map Analysis

Create **Frequency Maps** by computing the fundamental frequencies of orbits.

Regular motion: The computed frequencies do not vary in time

Chaotic motion: The computed frequencies vary in time



Steier et al., Phys. Rev. E (2002)

Papaphilippou & Laskar, Astron. Astrophys. (1998)

Chaos detection techniques

- **Based on the visualization of orbits**
 - ✓ Poincaré Surface of Section (PSS)
 - ✓ the color and rotation (CR) method
 - ✓ the 3D phase space slices (3PSS) technique
- **Based on the numerical analysis of orbits**
 - ✓ Frequency Map Analysis
 - ✓ 0-1 test
- **Chaos indicators based on the evolution of deviation vectors from a given orbit**
 - ✓ Maximum Lyapunov Exponent (MLE)
 - ✓ Fast Lyapunov Indicator (FLI) and Orthogonal Fast Lyapunov Indicators (OFLI and OFLI2)
 - ✓ Mean Exponential Growth Factor of Nearby Orbits (MEGNO)
 - ✓ Relative Lyapunov Indicator (RLI)
 - ✓ **Smaller ALignment Index – SALI**
 - ✓ **Generalized ALignment Index – GALI**

Maximum Lyapunov Exponent (MLE)

Chaos: sensitive dependence on initial conditions.

Roughly speaking, the MLE of a given orbit characterizes the **mean exponential rate of divergence** of trajectories surrounding it.

Consider an orbit in the $2N$ -dimensional phase space with **initial condition $x(0)$** and **an initial deviation vector (small perturbation) from it $v(0)$** .

Then the mean exponential rate of divergence is:

$$\text{MLE} = \lambda_1 = \lim_{t \rightarrow \infty} \Lambda(t) = \lim_{t \rightarrow \infty} \frac{1}{t} \ln \frac{\|v(t)\|}{\|v(0)\|}$$

$\lambda_1 = 0 \rightarrow$ Regular motion ($\Lambda \propto t^{-1}$)

$\lambda_1 > 0 \rightarrow$ Chaotic motion

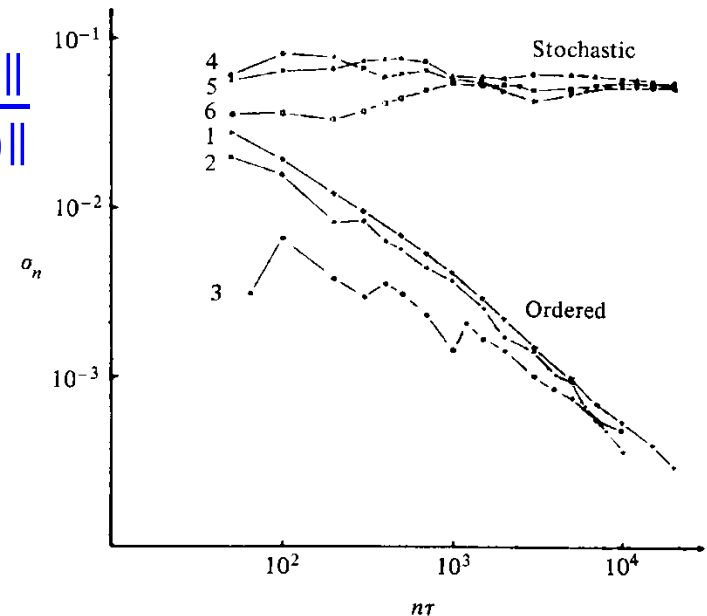


Figure 5.7. Behavior of σ_n at the intermediate energy $E = 0.125$ for initial points taken in the ordered (curves 1–3) or stochastic (curves 4–6) regions (after Benettin *et al.*, 1976).

**The
Smaller ALignment Index
(SALI)
method**

Definition of the SALI

We follow the evolution in time of two different initial deviation vectors ($\mathbf{v}_1(0)$, $\mathbf{v}_2(0)$), and define SALI [S., J. Phys. A (2001) – S. & Manos, Lect. Notes Phys. (2016)] as:

$$\text{SALI}(\mathbf{t}) = \min\{\|\hat{\mathbf{v}}_1(\mathbf{t}) + \hat{\mathbf{v}}_2(\mathbf{t})\|, \|\hat{\mathbf{v}}_1(\mathbf{t}) - \hat{\mathbf{v}}_2(\mathbf{t})\|\}$$

where

$$\hat{\mathbf{v}}_1(\mathbf{t}) = \frac{\mathbf{v}_1(\mathbf{t})}{\|\mathbf{v}_1(\mathbf{t})\|}$$

When the two vectors become collinear

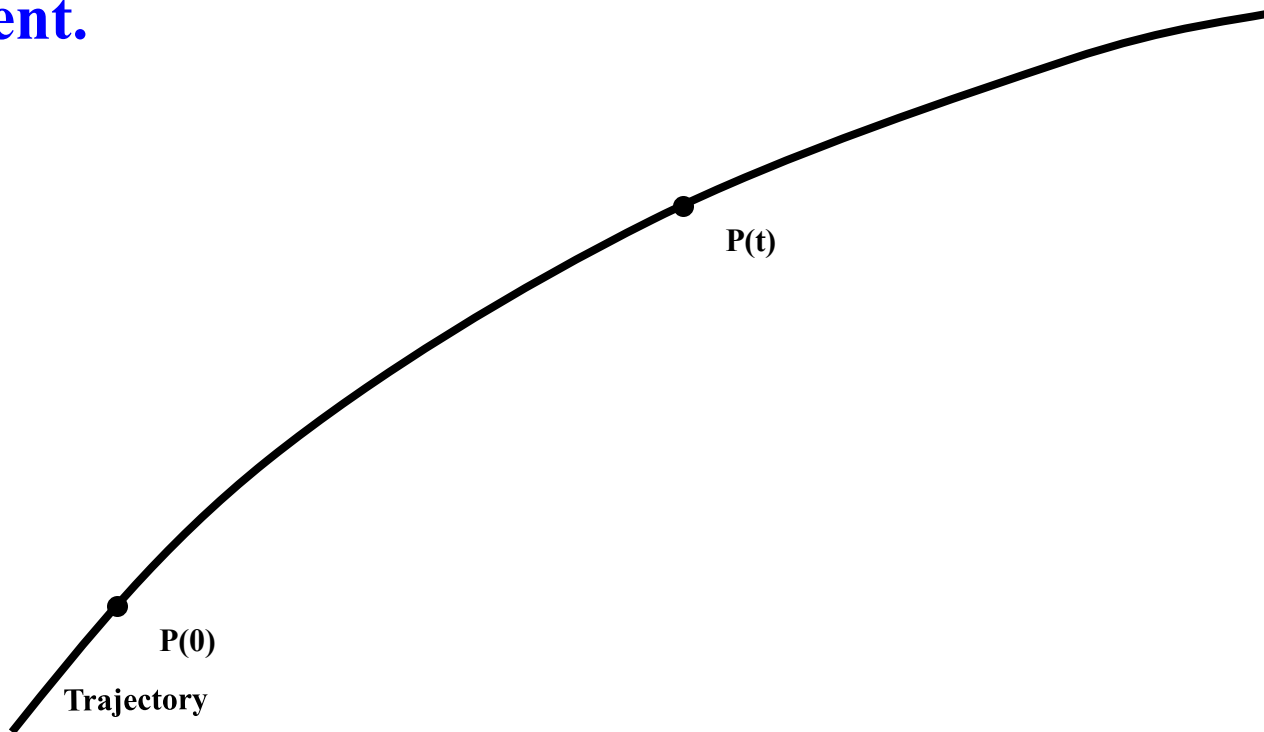
$$\text{SALI}(\mathbf{t}) \rightarrow 0$$

Behavior of SALI for **chaotic motion**

For chaotic orbits the two initially different deviation vectors tend to coincide with the direction defined by the maximum Lyapunov exponent.

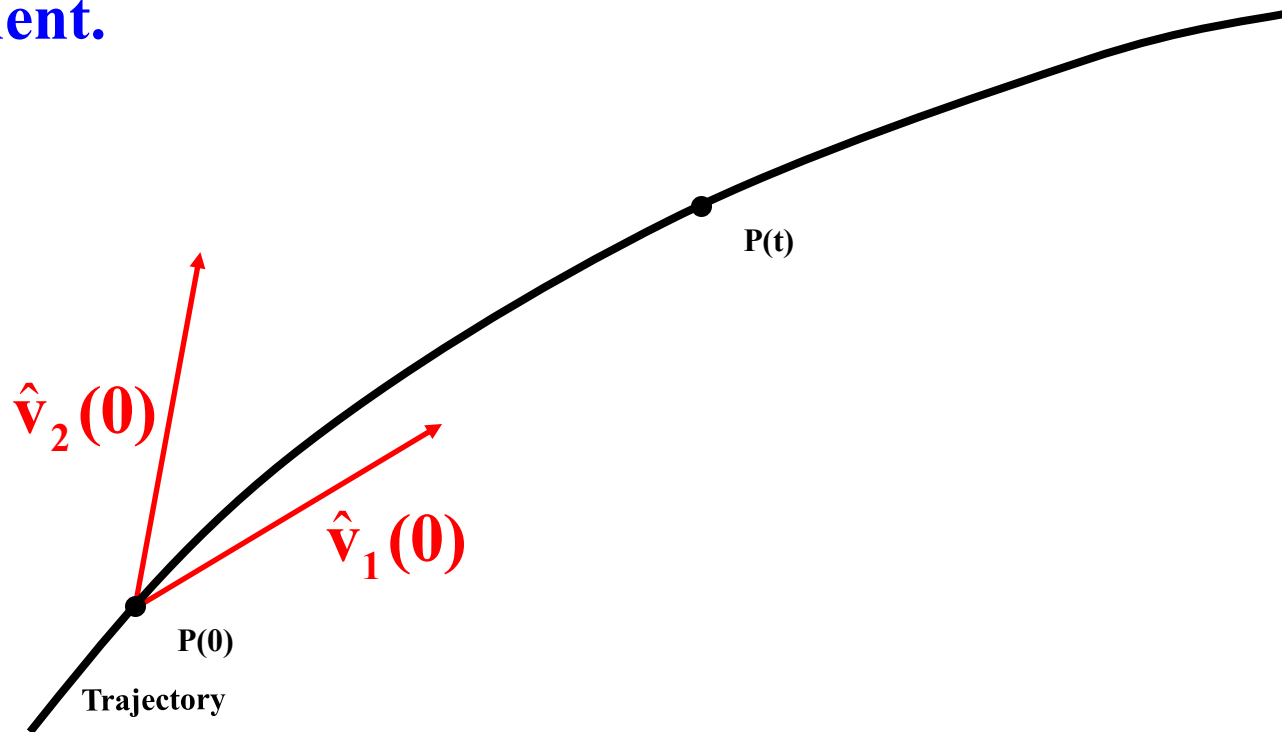
Behavior of SALI for **chaotic motion**

For chaotic orbits the two initially different deviation vectors tend to coincide with the direction defined by the maximum Lyapunov exponent.



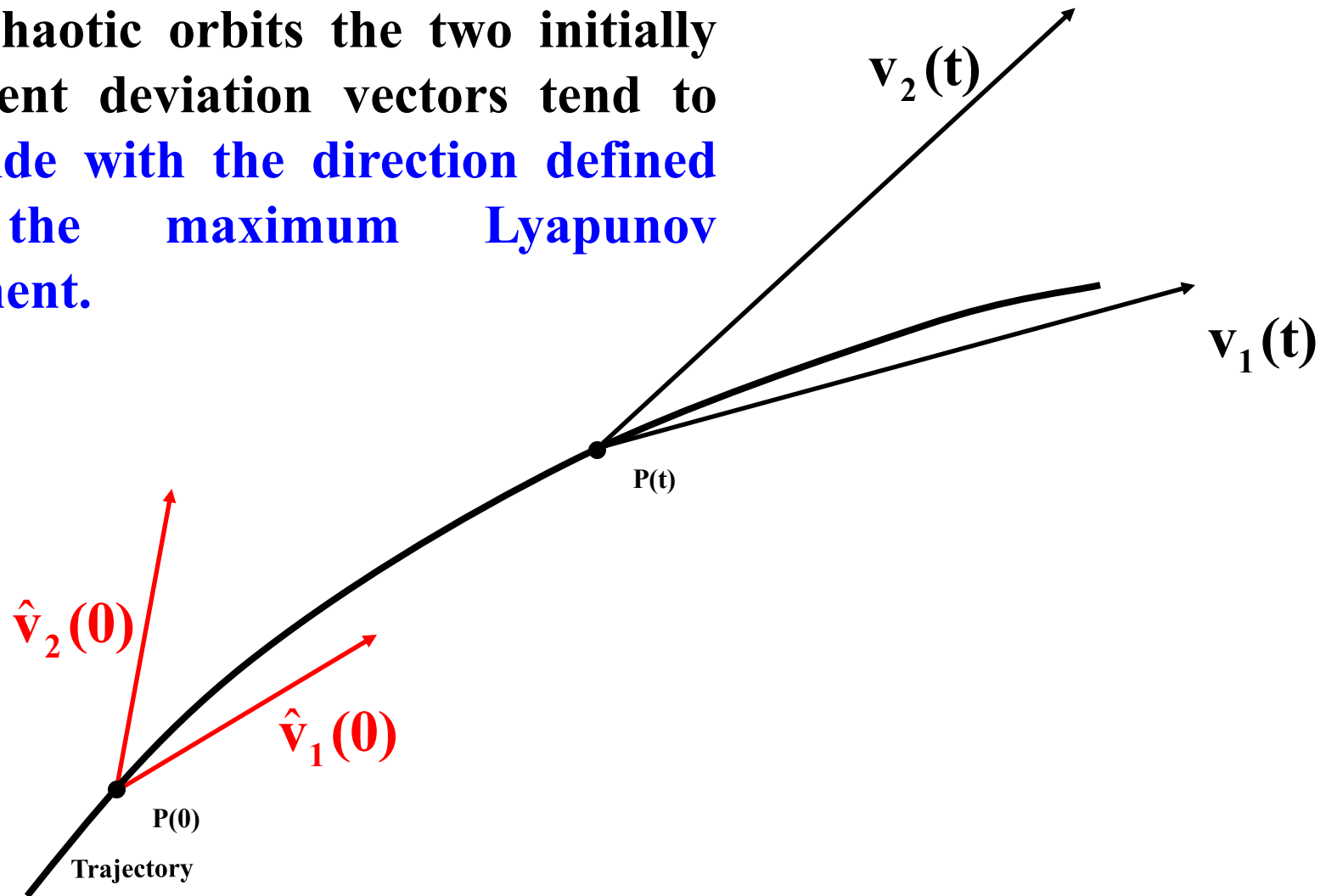
Behavior of SALI for **chaotic motion**

For chaotic orbits the two initially different deviation vectors tend to coincide with the direction defined by the maximum Lyapunov exponent.



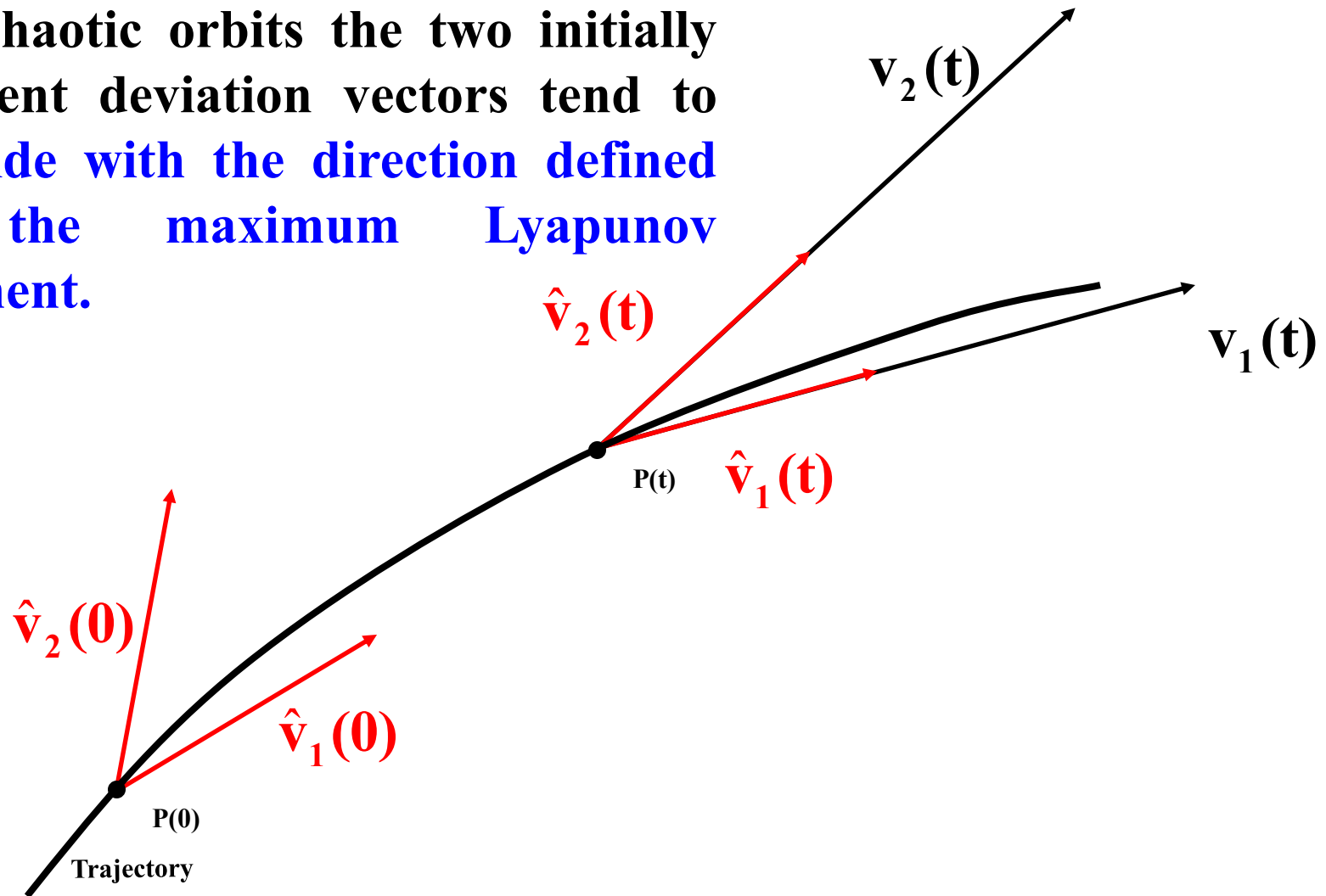
Behavior of SALI for **chaotic motion**

For chaotic orbits the two initially different deviation vectors tend to coincide with the direction defined by the maximum Lyapunov exponent.



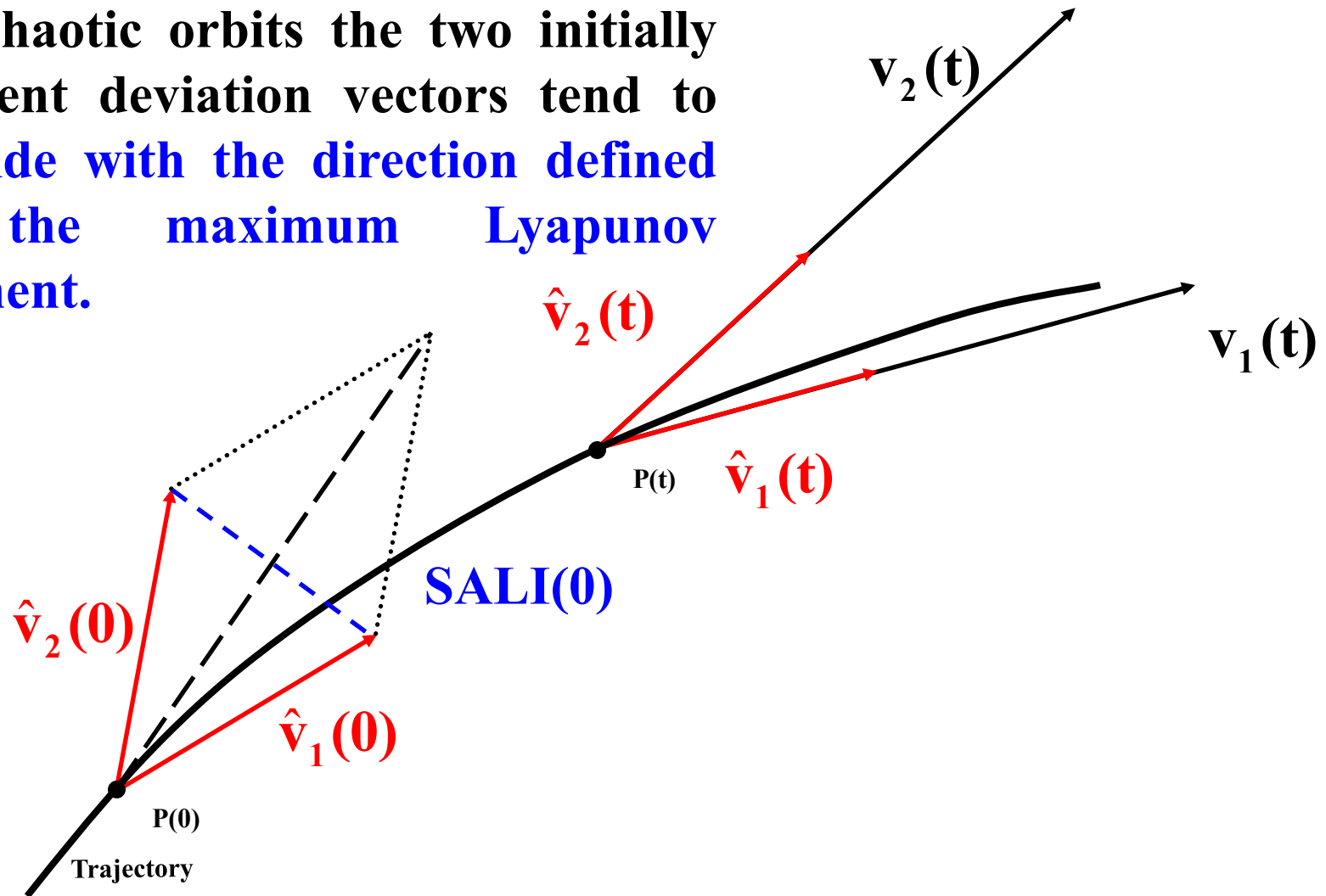
Behavior of SALI for **chaotic motion**

For chaotic orbits the two initially different deviation vectors tend to coincide with the direction defined by the maximum Lyapunov exponent.



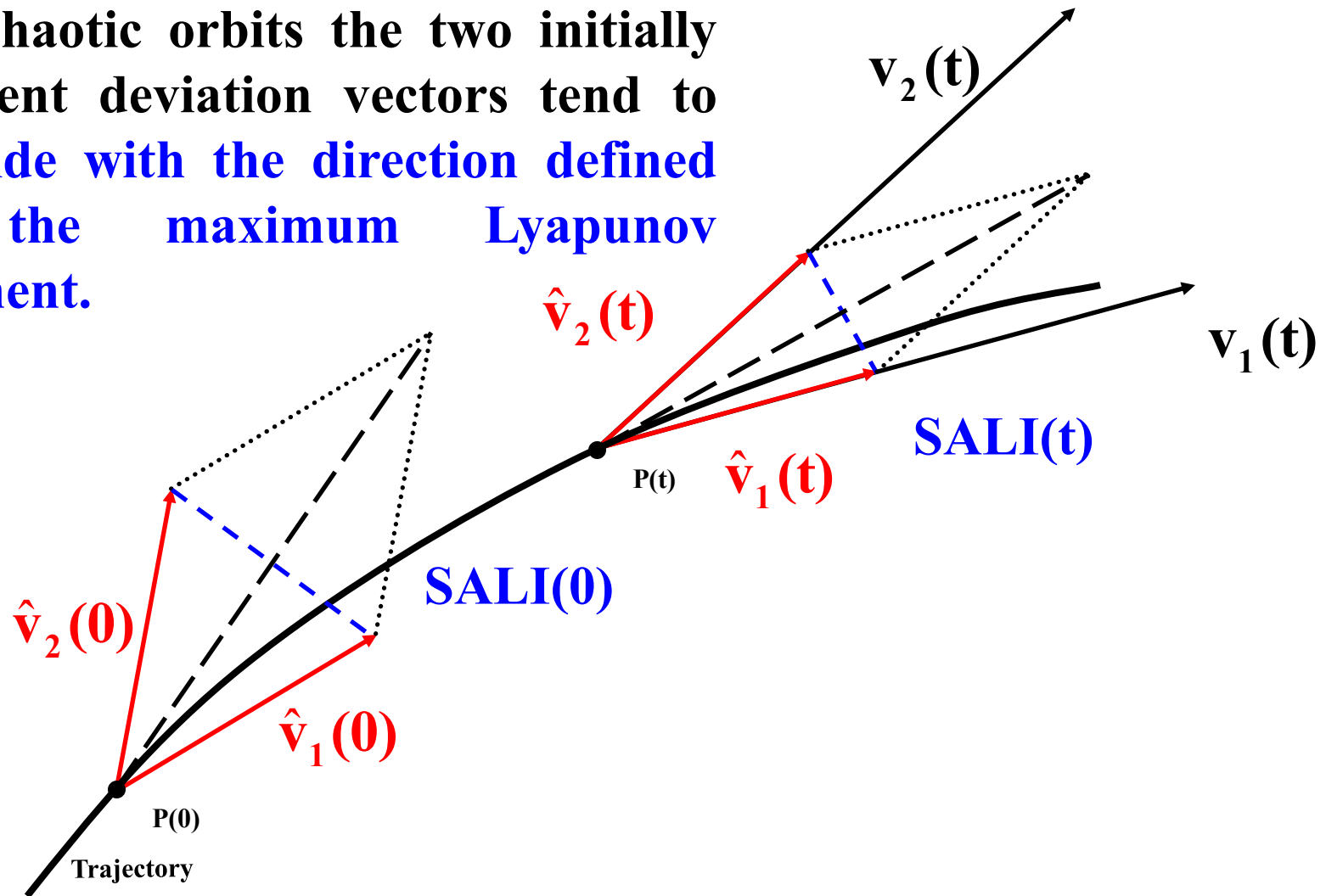
Behavior of SALI for **chaotic motion**

For chaotic orbits the two initially different deviation vectors tend to coincide with the direction defined by the maximum Lyapunov exponent.



Behavior of SALI for **chaotic motion**

For chaotic orbits the two initially different deviation vectors tend to coincide with the direction defined by the maximum Lyapunov exponent.

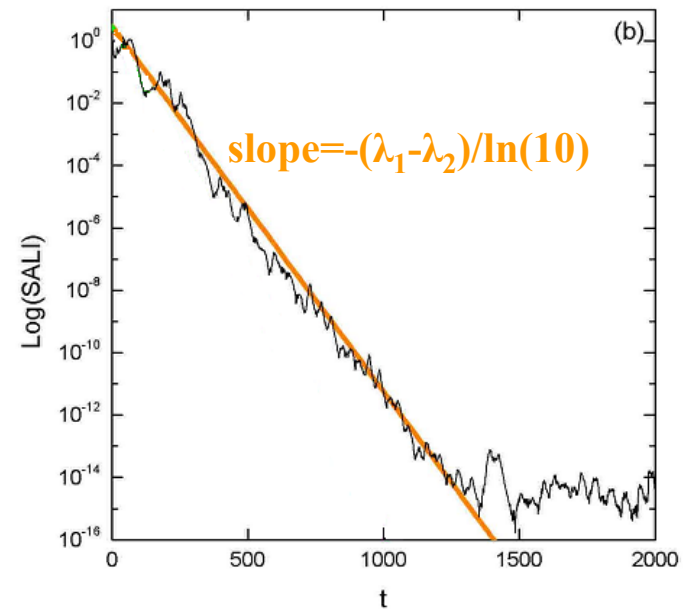
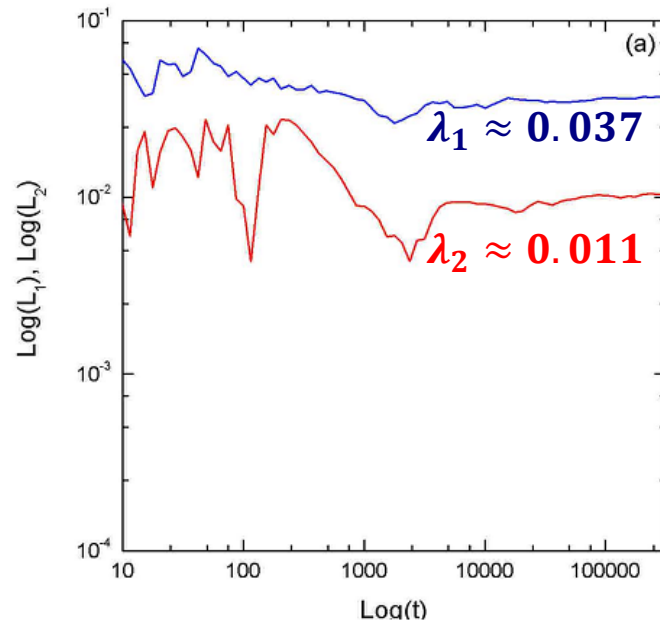


Behavior of the SALI for **chaotic motion**

We test the validity of the approximation $\text{SALI} \propto e^{-(\lambda_1 - \lambda_2)t}$ [S. et al., J. Phys. A (2004)] for a chaotic orbit of the 3D Hamiltonian

$$H = \sum_{i=1}^3 \frac{\omega_i}{2} (q_i^2 + p_i^2) + q_1^2 q_2 + q_1^2 q_3$$

with $\omega_1=1$, $\omega_2=1.4142$, $\omega_3=1.7321$, $H=0.09$

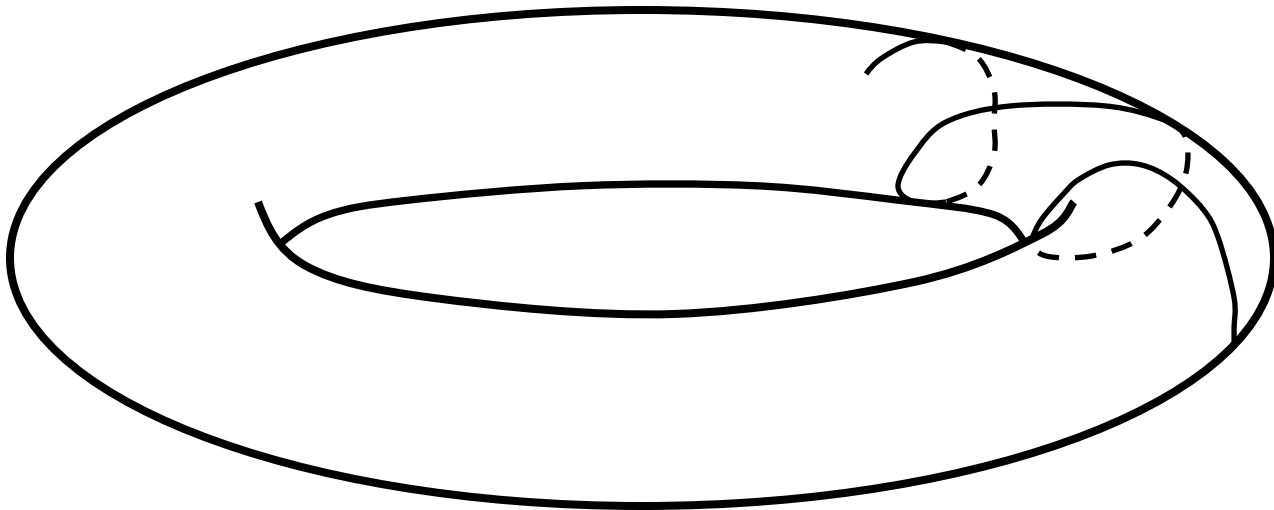


Behavior of SALI for **regular motion**

Regular motion occurs on a torus and two different initial deviation vectors **become tangent to the torus, generally having different directions.**

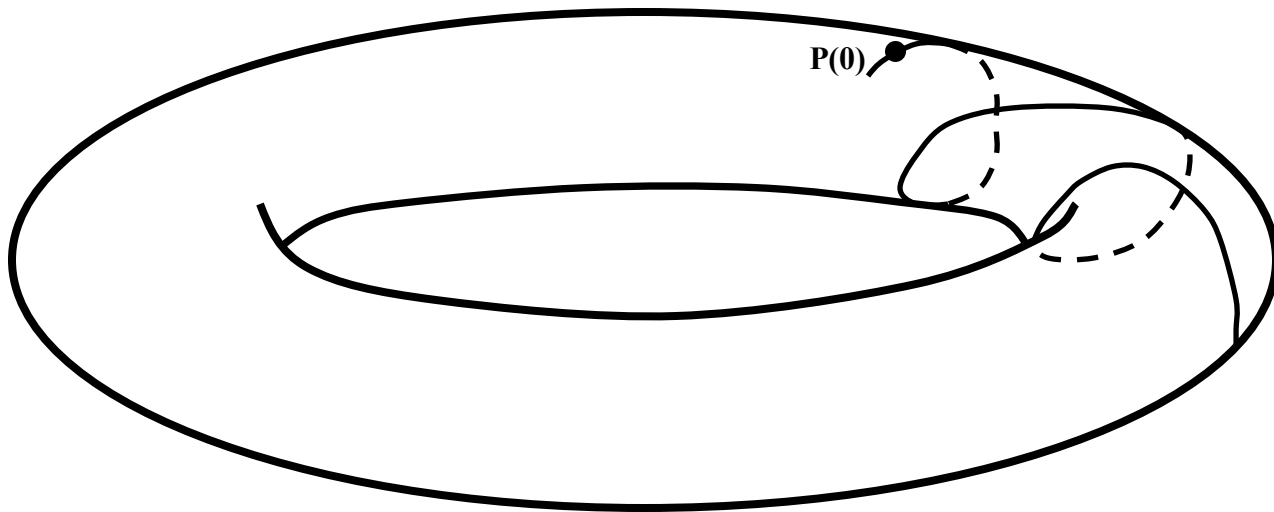
Behavior of SALI for **regular motion**

Regular motion occurs on a torus and two different initial deviation vectors **become tangent to the torus, generally having different directions.**



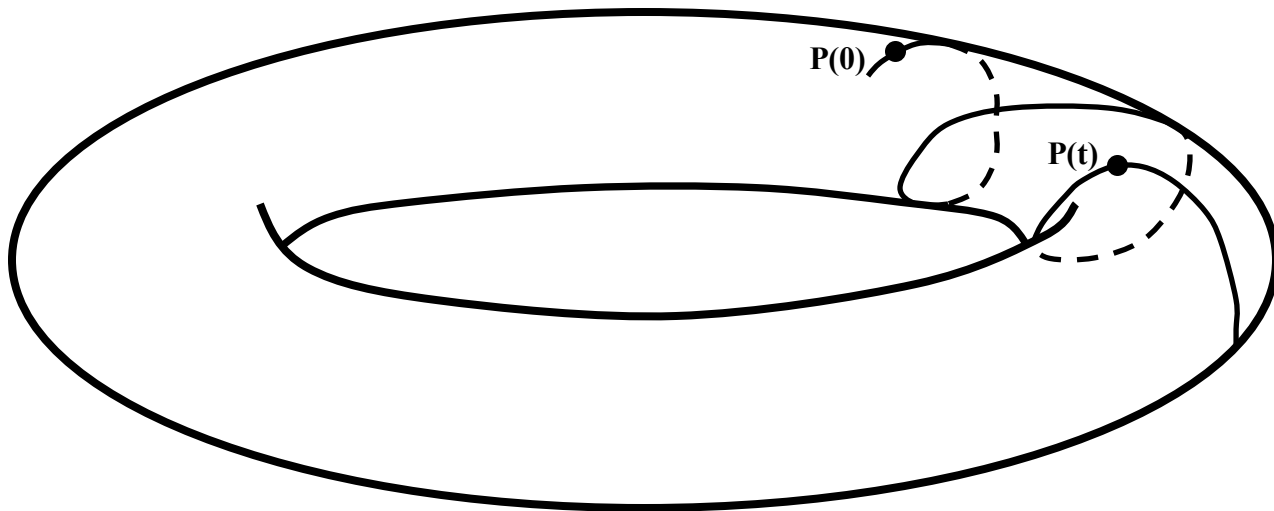
Behavior of SALI for **regular motion**

Regular motion occurs on a torus and two different initial deviation vectors **become tangent to the torus, generally having different directions.**



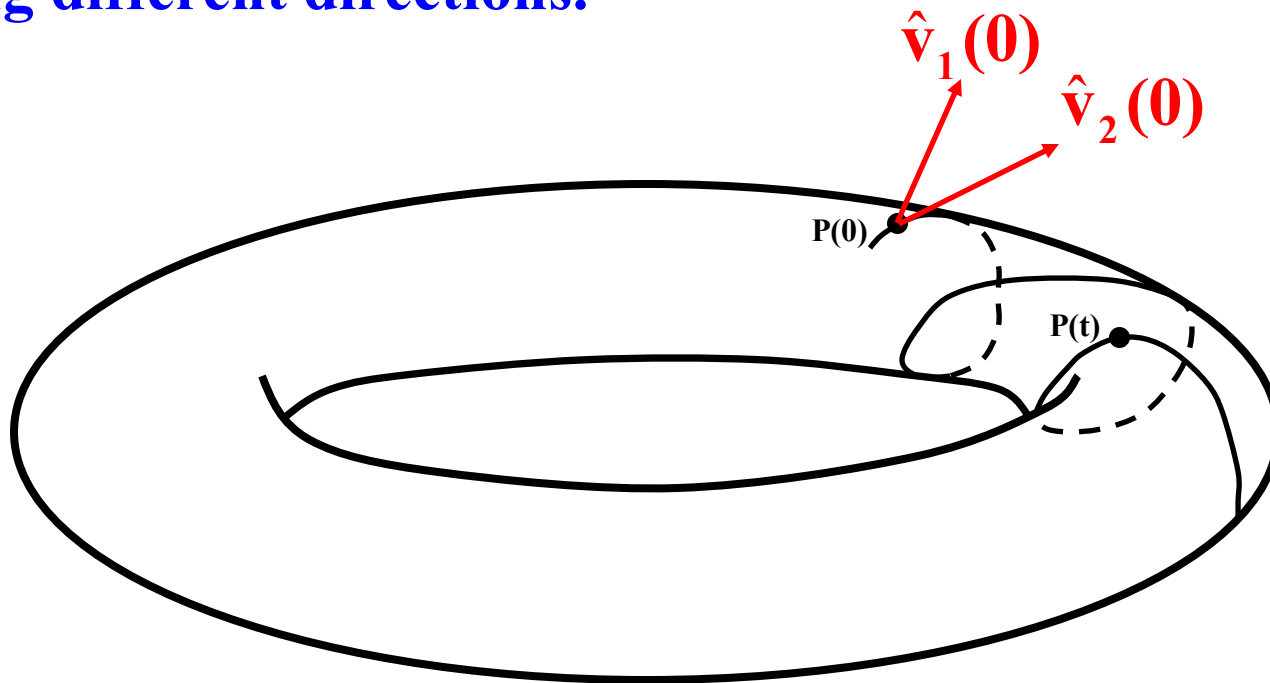
Behavior of SALI for **regular motion**

Regular motion occurs on a torus and two different initial deviation vectors **become tangent to the torus, generally having different directions.**



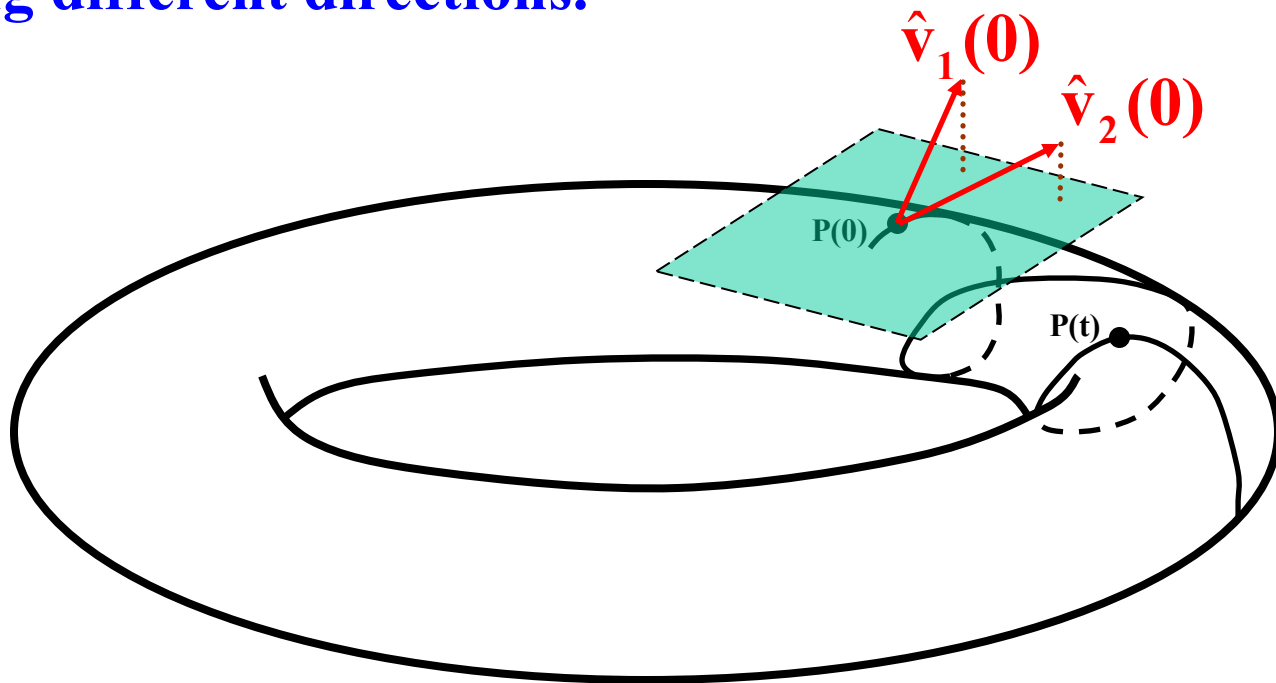
Behavior of SALI for **regular motion**

Regular motion occurs on a torus and two different initial deviation vectors **become tangent to the torus, generally having different directions.**



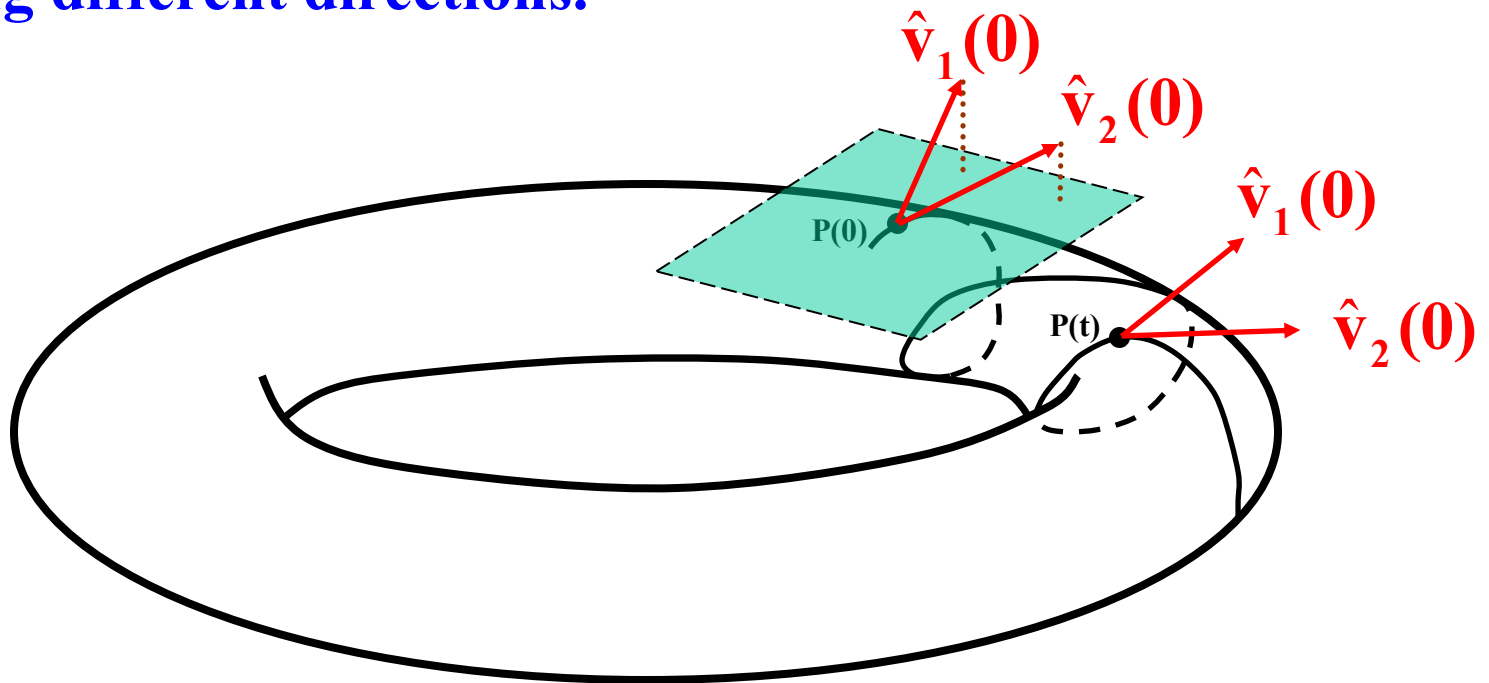
Behavior of SALI for **regular motion**

Regular motion occurs on a torus and two different initial deviation vectors **become tangent to the torus**, generally **having different directions**.



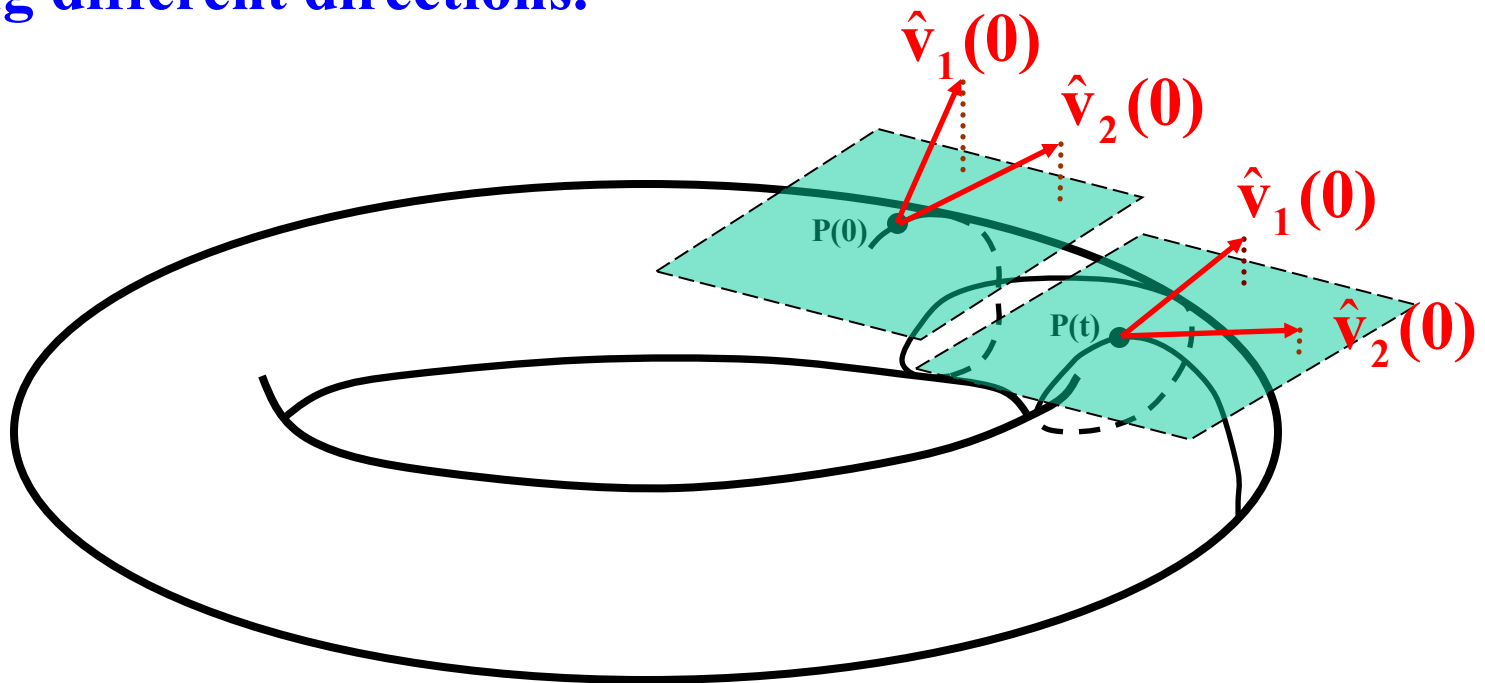
Behavior of SALI for **regular motion**

Regular motion occurs on a torus and two different initial deviation vectors **become tangent to the torus, generally having different directions.**



Behavior of SALI for **regular motion**

Regular motion occurs on a torus and two different initial deviation vectors **become tangent to the torus**, generally **having different directions**.



SALI – Hénon-Heiles system

As an example, we consider the 2D Hénon-Heiles system:

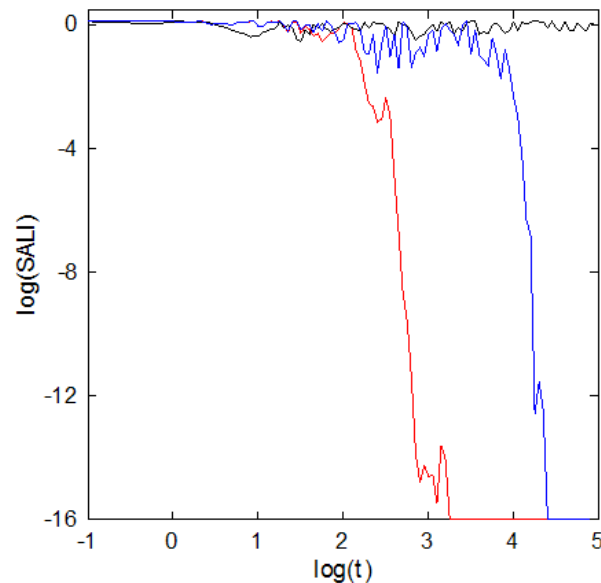
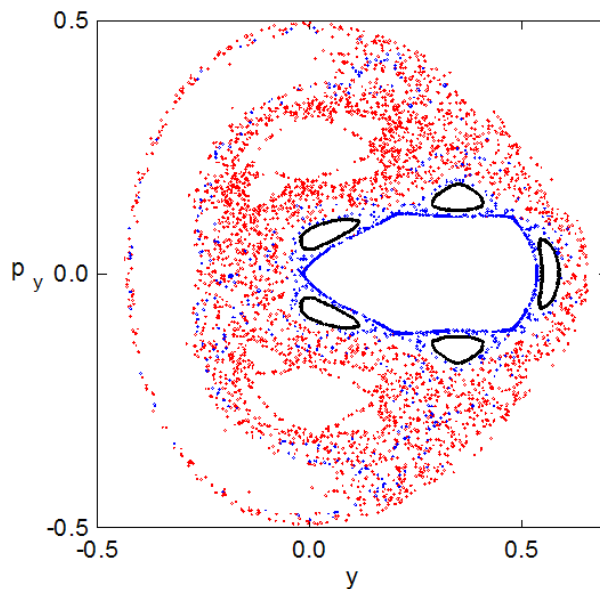
$$H = \frac{1}{2}(p_x^2 + p_y^2) + \frac{1}{2}(x^2 + y^2) + x^2y - \frac{1}{3}y^3$$

For $E=1/8$ we consider the orbits with initial conditions:

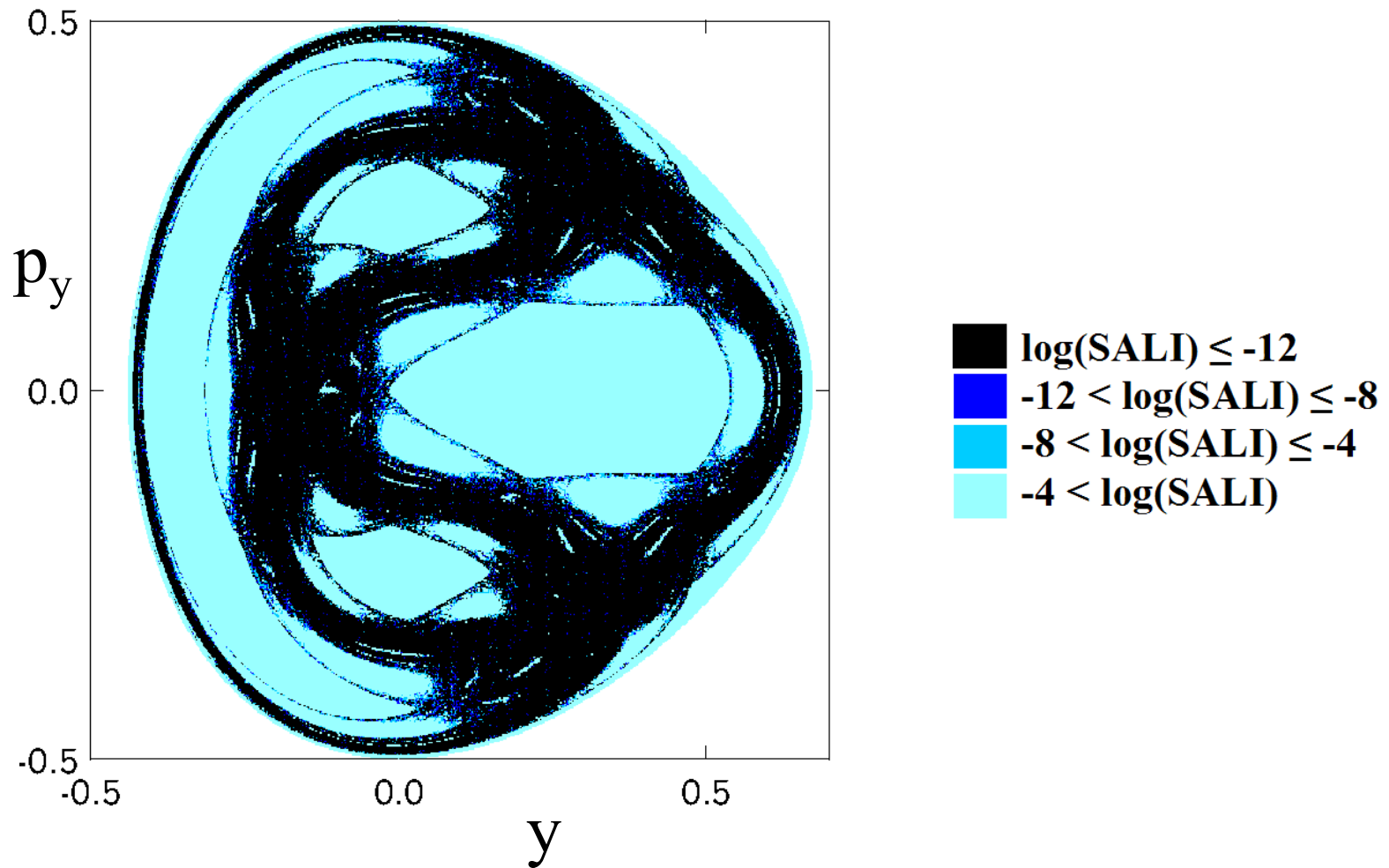
Regular orbit, $x=0$, $y=0.55$, $p_x=0.2417$, $p_y=0$

Chaotic orbit, $x=0$, $y=-0.016$, $p_x=0.49974$, $p_y=0$

Chaotic orbit, $x=0$, $y=-0.01344$, $p_x=0.49982$, $p_y=0$



SALI – Hénon-Heiles system



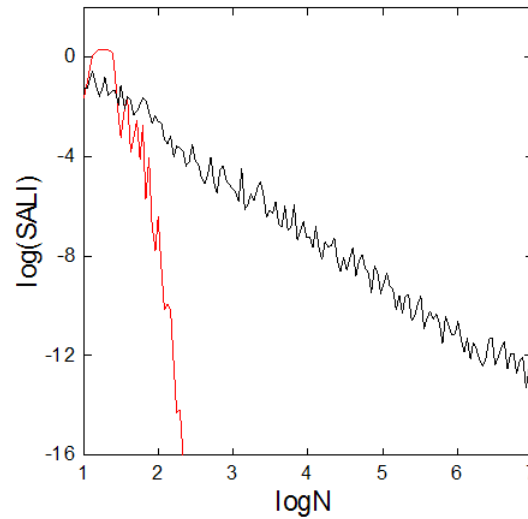
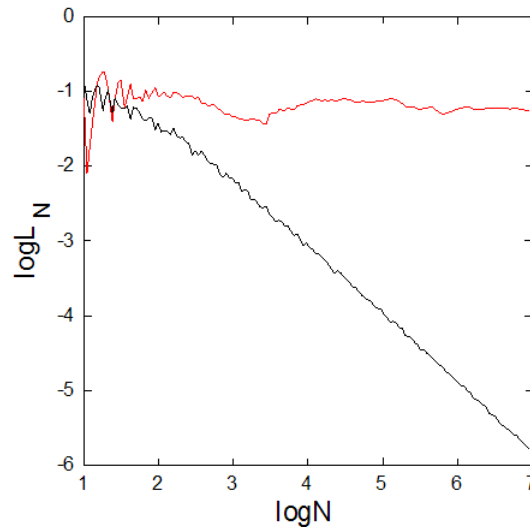
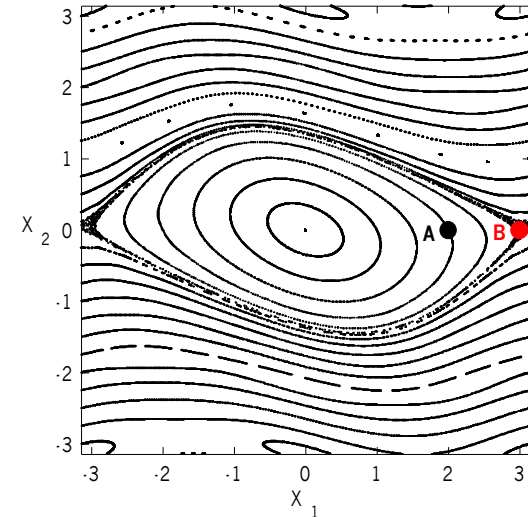
Applications – 2D map

$$\begin{aligned}x_1' &= x_1 + x_2 \\x_2' &= x_2 - \nu \sin(x_1 + x_2)\end{aligned}\quad (\text{mod } 2\pi)$$

For $\nu=0.5$ we consider the orbits:

regular orbit A with initial conditions $x_1=2, x_2=0$.

chaotic orbit B with initial conditions $x_1=3, x_2=0$.



Behavior of the SALI

2D maps

SALI $\rightarrow 0$ both for regular and chaotic orbits

following, however, completely different time rates which allows us to distinguish between the two cases.

Hamiltonian flows and multidimensional maps

SALI $\rightarrow 0$ for chaotic orbits

SALI $\rightarrow \text{constant} \neq 0$ for regular orbits

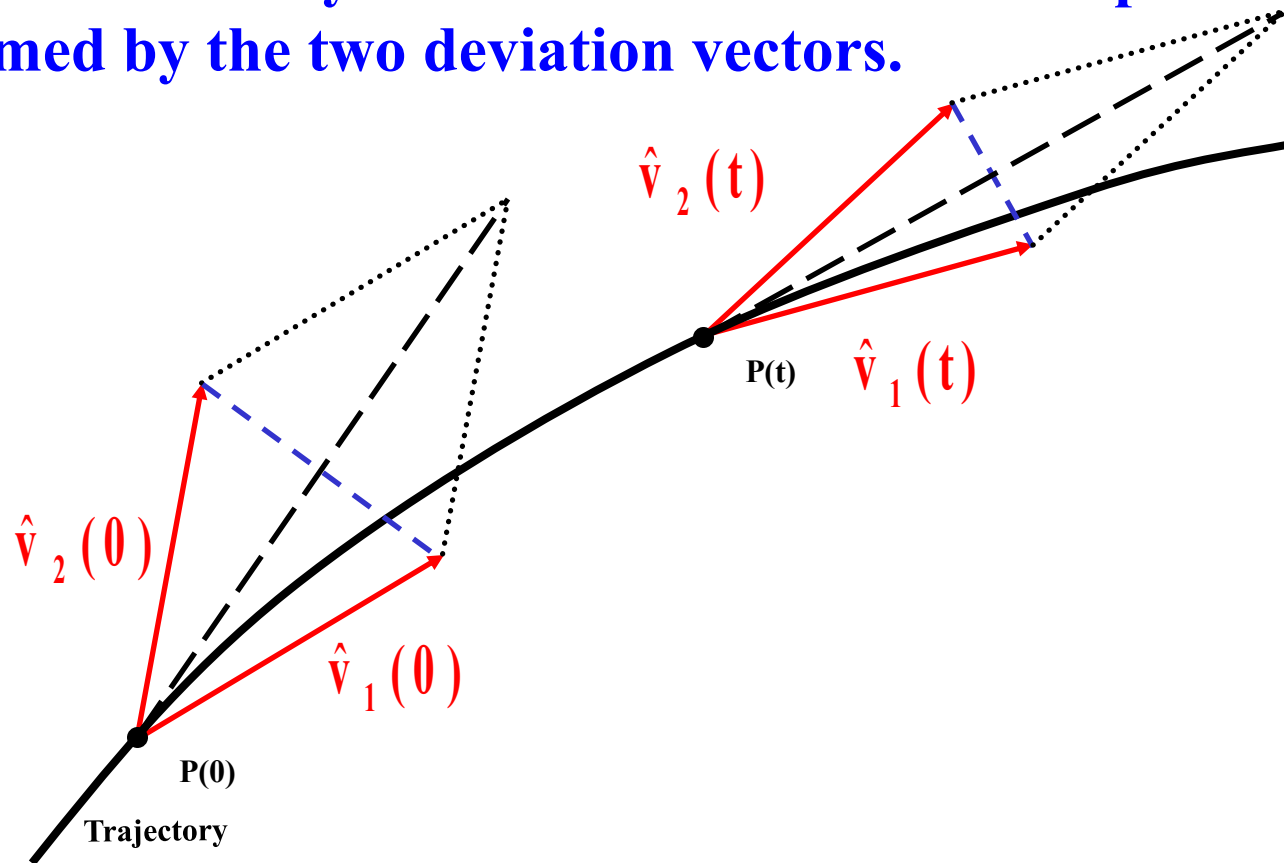
The Generalized ALignment Indices (GALIs) method

Definition of the Generalized Alignment Index (GALI)

SALI effectively measures the 'area' of the parallelogram formed by the two deviation vectors.

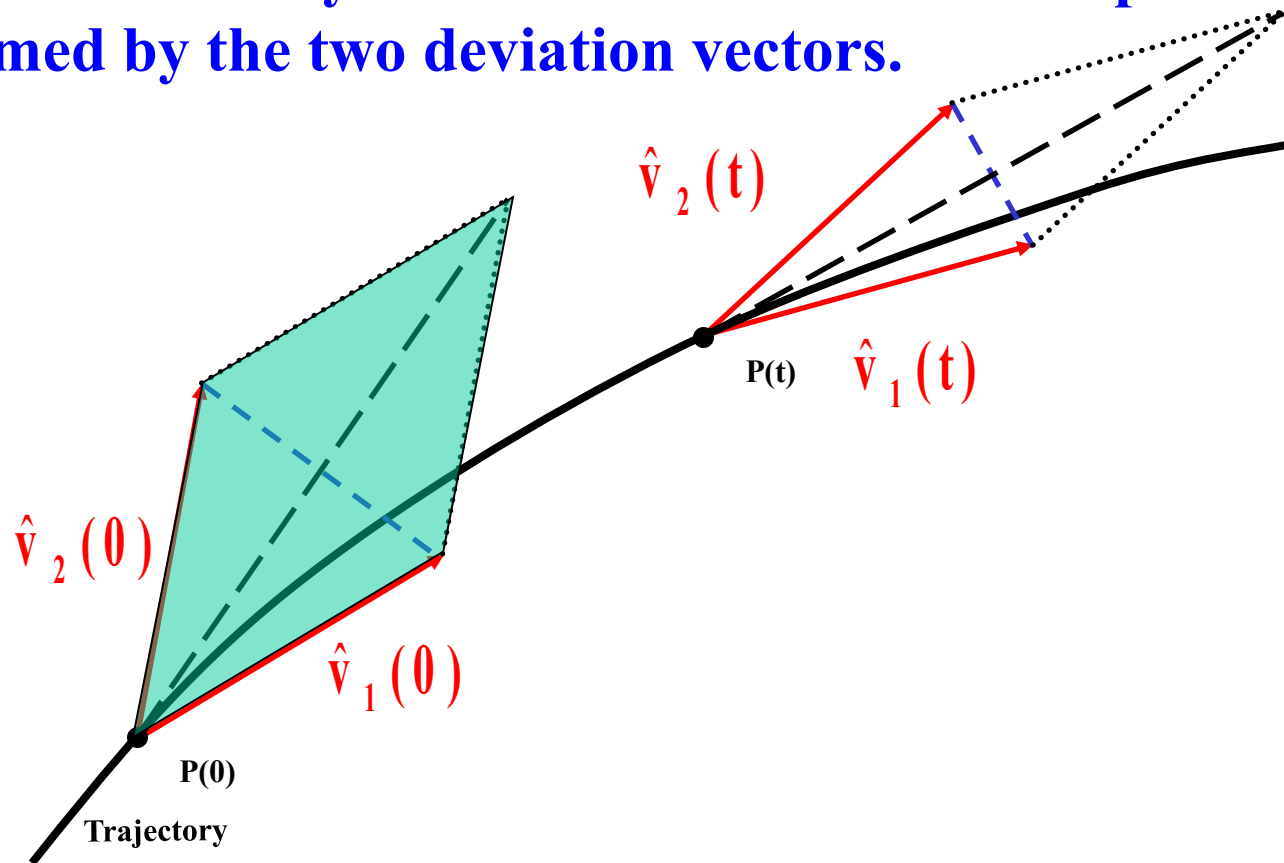
Definition of the Generalized Alignment Index (GALI)

SALI effectively measures the 'area' of the parallelogram formed by the two deviation vectors.



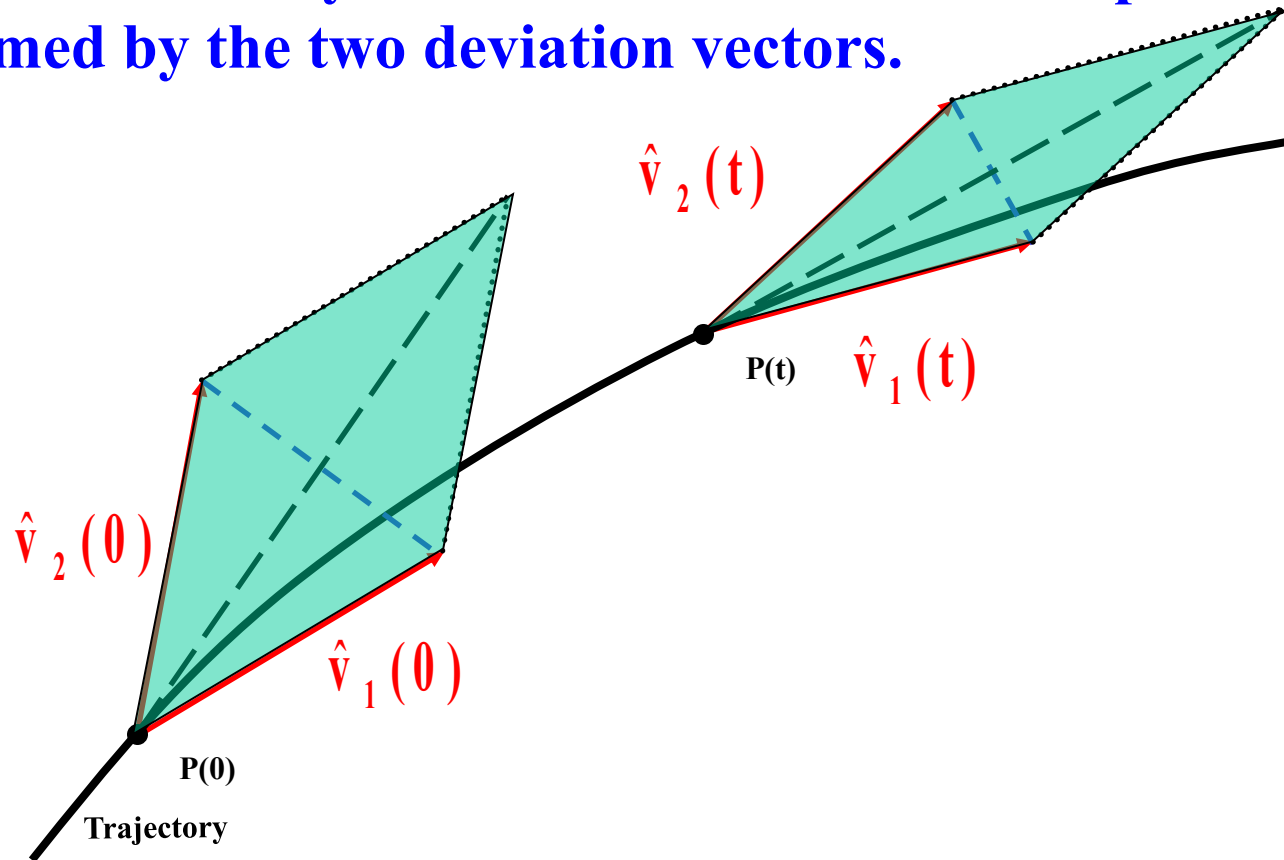
Definition of the Generalized Alignment Index (GALI)

SALI effectively measures the 'area' of the parallelogram formed by the two deviation vectors.



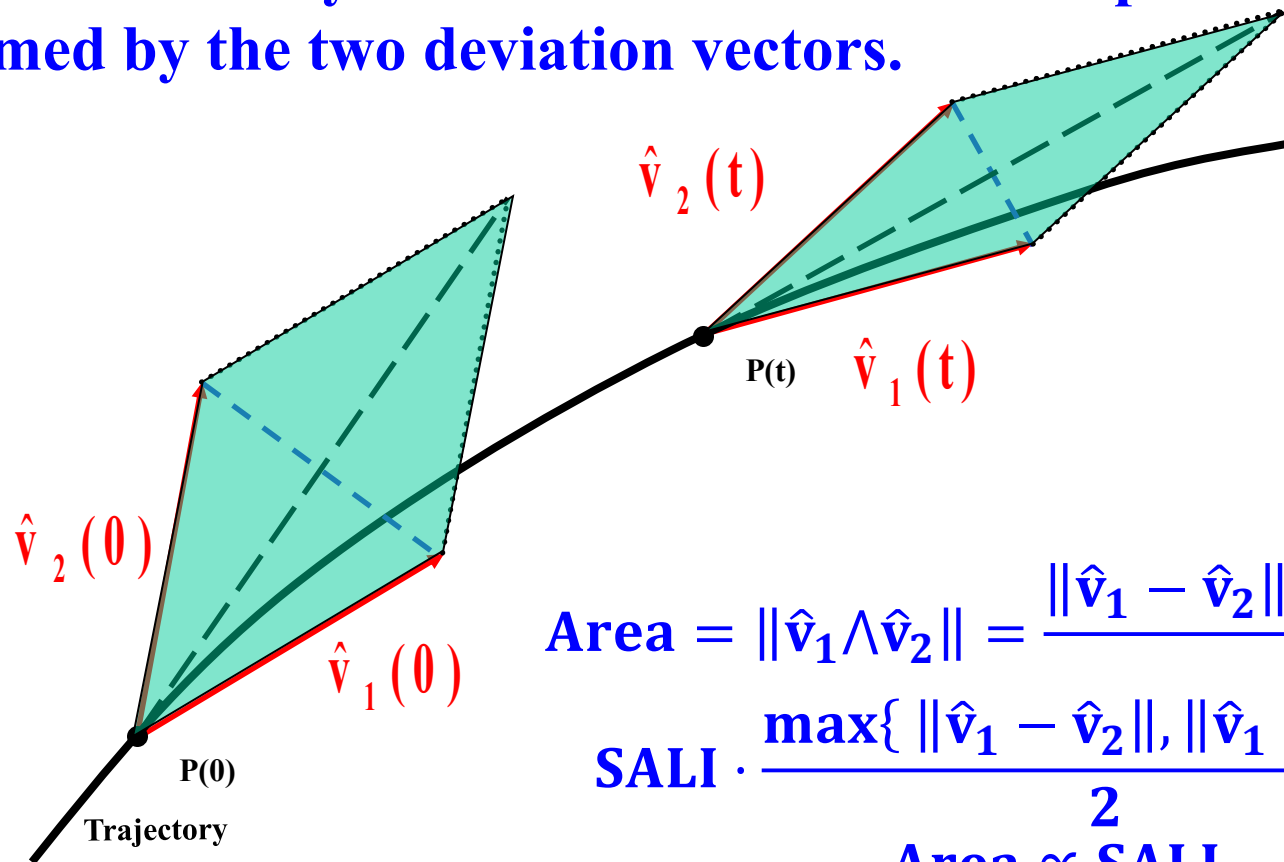
Definition of the Generalized Alignment Index (GALI)

SALI effectively measures the 'area' of the parallelogram formed by the two deviation vectors.



Definition of the Generalized Alignment Index (GALI)

SALI effectively measures the ‘area’ of the parallelogram formed by the two deviation vectors.



$$\text{Area} = \|\hat{\mathbf{v}}_1 \wedge \hat{\mathbf{v}}_2\| = \frac{\|\hat{\mathbf{v}}_1 - \hat{\mathbf{v}}_2\| \cdot \|\hat{\mathbf{v}}_1 + \hat{\mathbf{v}}_2\|}{2} =$$

$$\text{SALI} \cdot \frac{\max\{\|\hat{\mathbf{v}}_1 - \hat{\mathbf{v}}_2\|, \|\hat{\mathbf{v}}_1 + \hat{\mathbf{v}}_2\|\}}{2} \Rightarrow$$

$$\text{Area} \propto \text{SALI}$$

Definition of the Generalized Alignment Index (GALI)

In the case of an N degree of freedom Hamiltonian system we follow the evolution of k deviation vectors with $2 \leq k \leq 2N$, and define [S. et al., Physica D (2007)] the Generalized Alignment Index (GALI) of order k :

$$\text{GALI}_k(t) = \|\hat{\mathbf{v}}_1(t) \wedge \hat{\mathbf{v}}_2(t) \wedge \dots \wedge \hat{\mathbf{v}}_k(t)\|$$

where

$$\hat{\mathbf{v}}_1(t) = \frac{\mathbf{v}_1(t)}{\|\mathbf{v}_1(t)\|}.$$

Note that GALI_2 ($k=2$) is equivalent to the Smaller Alignment Index (SALI).

Behavior of the GALI_k

Chaotic motion: GALI_k ($2 \leq k \leq 2N$) tends exponentially to zero with exponents which involve the values of the first k largest Lyapunov exponents $\lambda_1, \lambda_2, \dots, \lambda_k$:

$$\text{GALI}_k(t) \propto e^{-[(\lambda_1 - \lambda_2) + (\lambda_1 - \lambda_3) + \dots + (\lambda_1 - \lambda_k)]t}$$

Regular motion: When the motion occurs on an N -dimensional torus then the behavior of GALI_k is given by [S. et al., Physica D (2007) – S. et al., Eur. Phys. J. Sp. Top. (2008)]:

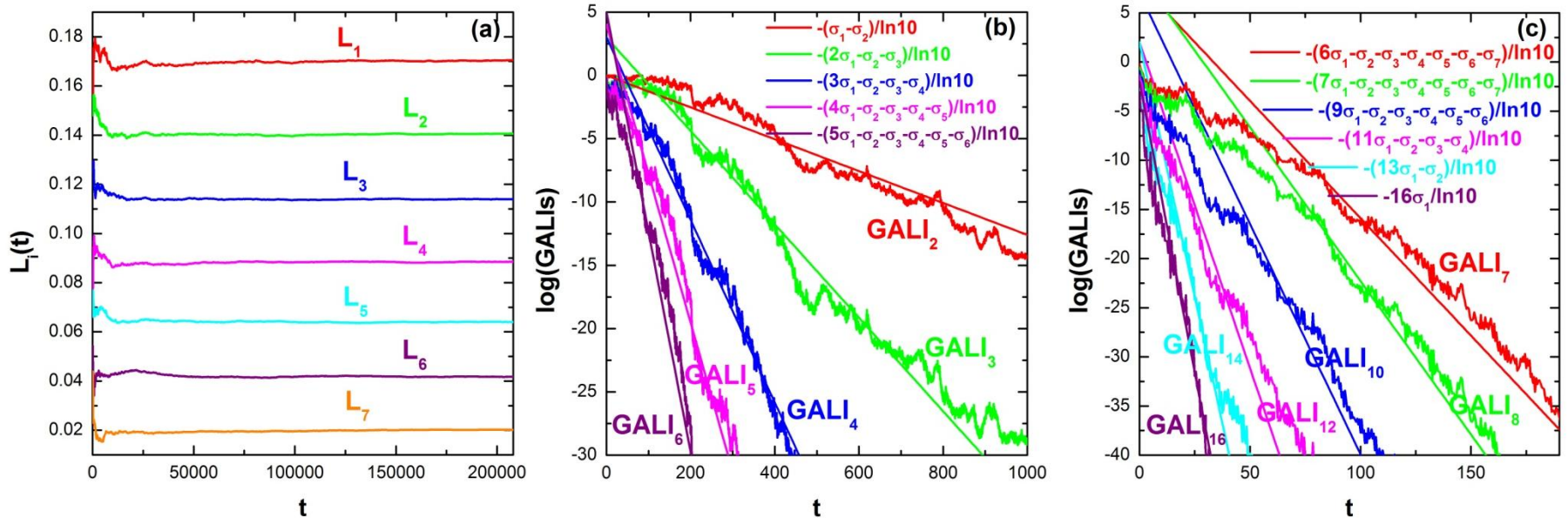
$$\text{GALI}_k(t) \propto \begin{cases} \text{constant} & \text{if } 2 \leq k \leq N \\ \frac{1}{t^{2(k-N)}} & \text{if } N < k \leq 2N \end{cases}$$

Behavior of the $GALI_k$ for **chaotic motion**

N particles Fermi-Pasta-Ulam-Tsingou (FPUT) system:

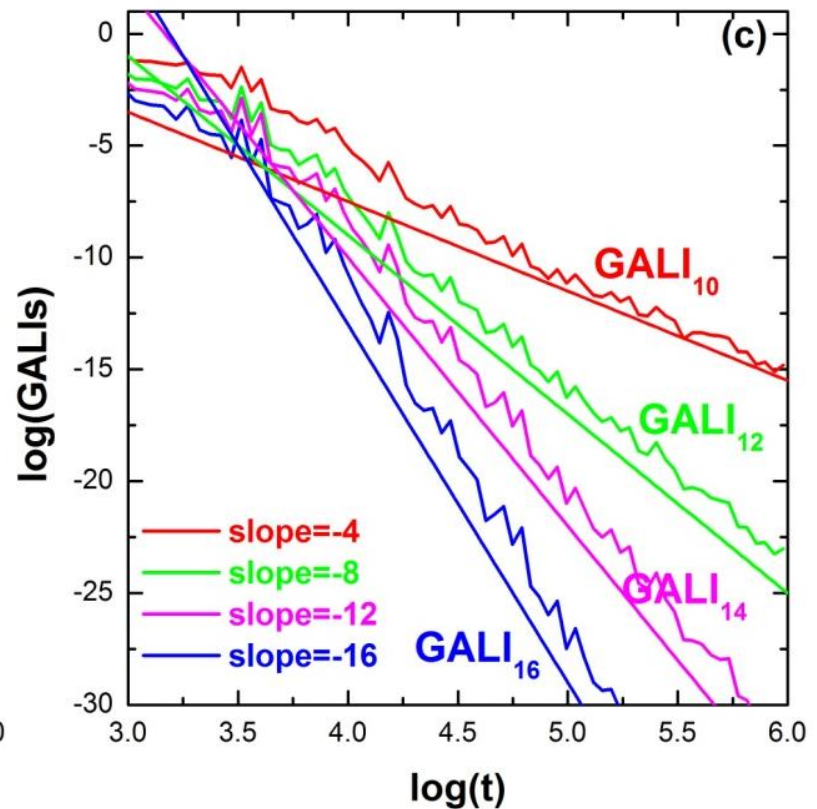
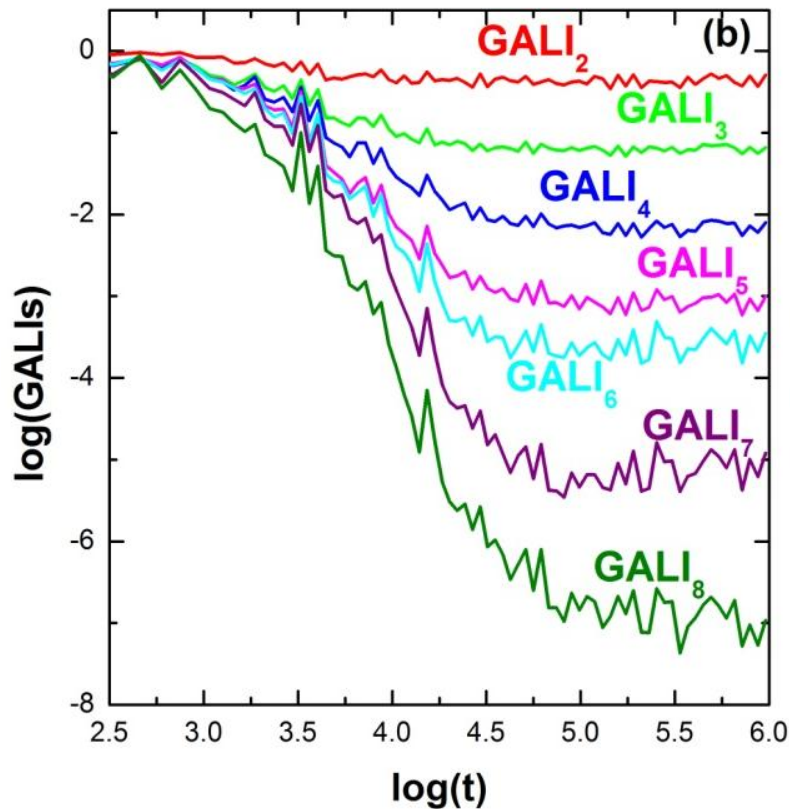
$$H = \frac{1}{2} \sum_{i=1}^N p_i^2 + \sum_{i=0}^N \left[\frac{1}{2} (q_{i+1} - q_i)^2 + \frac{\beta}{4} (q_{i+1} - q_i)^4 \right]$$

with fixed boundary conditions, $N=8$ and $\beta=1.5$.



Behavior of the $GALI_k$ for regular motion

N=8 FPUT system



Global dynamics

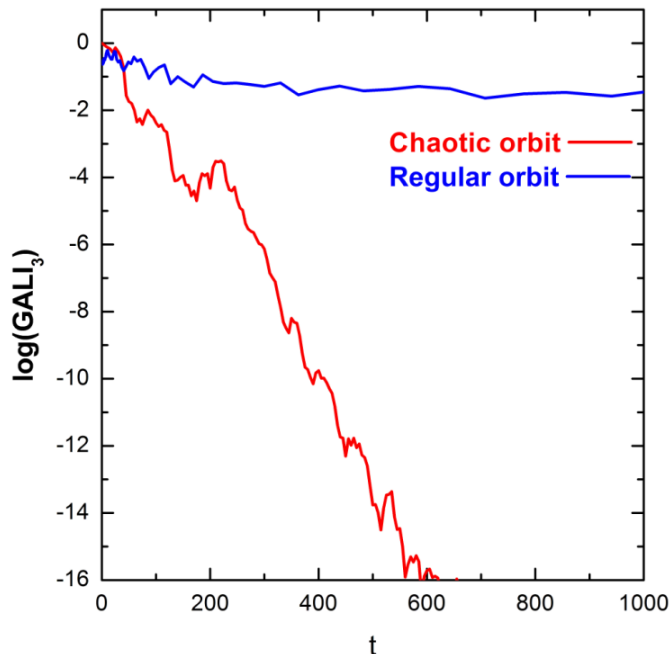
- GALI_2 (practically equivalent to the use of SALI)

- GALI_N

**Chaotic motion: $\text{GALI}_N \rightarrow 0$
(exponential decay)**

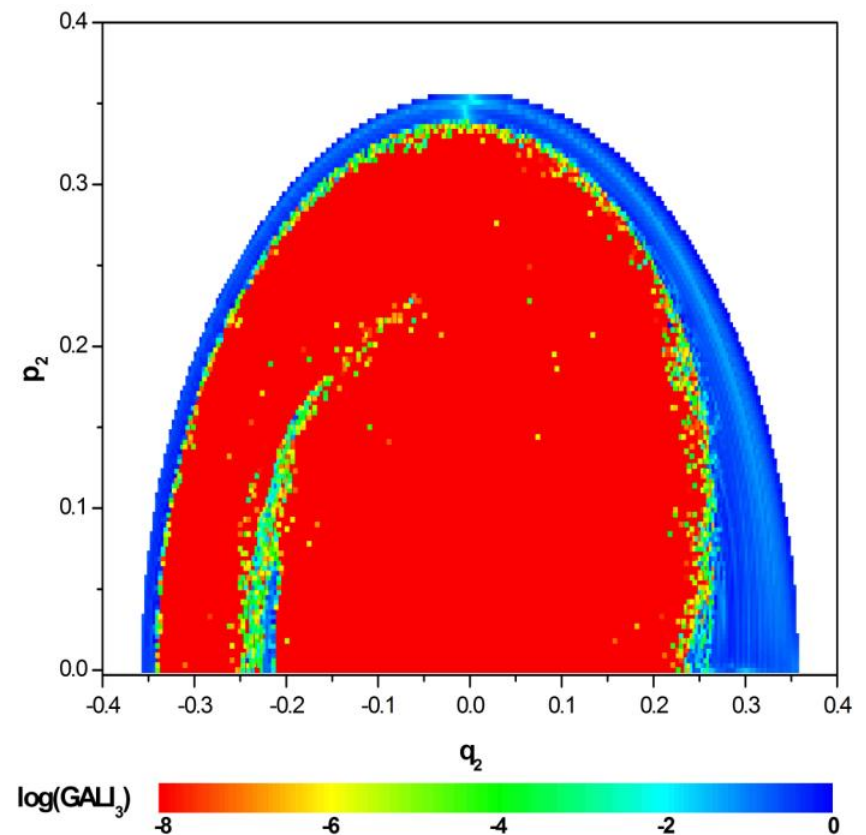
Regular motion:

$\text{GALI}_N \approx \text{constant} \neq 0$



3D Hamiltonian

Subspace $q_3=p_3=0$, $p_2 \geq 0$ for $t=1000$.



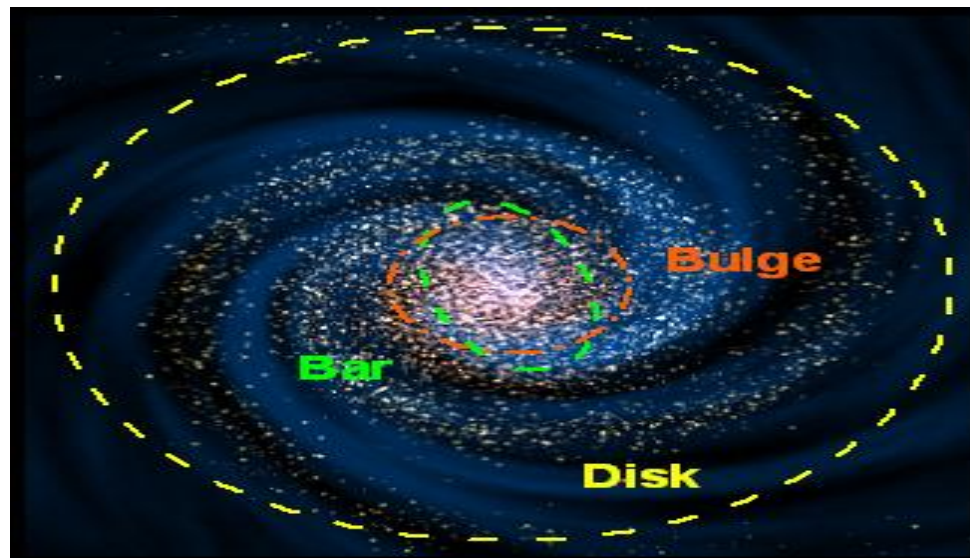
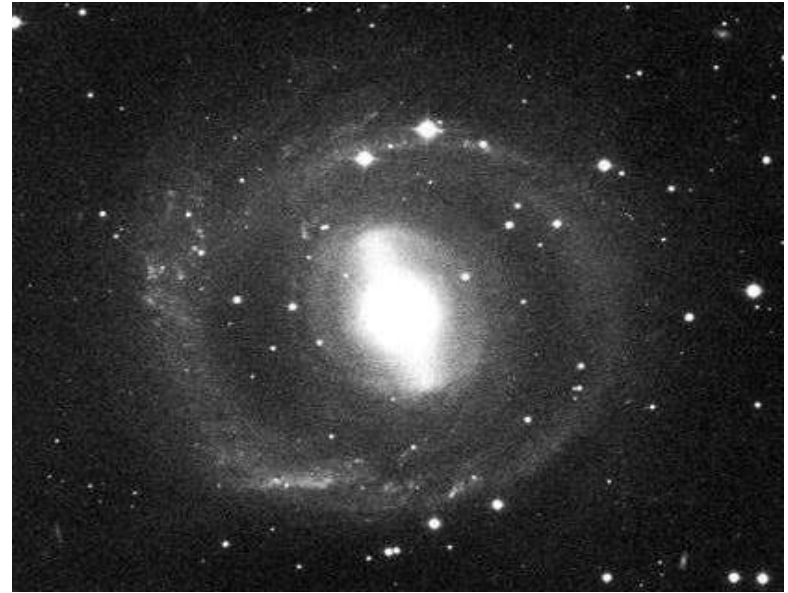
A time-dependent Hamiltonian system

Barred galaxies

NGC 1433



NGC 2217



Barred galaxy model

The 3D bar rotates around its short z -axis (x : long axis and y : intermediate). The Hamiltonian that describes the motion for this model is:

$$H = \frac{1}{2}(p_x^2 + p_y^2 + p_z^2) + V(x, y, z) - \Omega_b(xp_y - yp_x) \equiv \text{Energy}$$

This model consists of the superposition of potentials describing an **axisymmetric** part and a **bar** component of the galaxy [Manos et al., J. Phys. A (2013)].

a) Axisymmetric component:

i) **Plummer sphere:**

$$V_{\text{sphere}}(x, y, z) = -\frac{GM_S}{\sqrt{x^2 + y^2 + z^2 + \epsilon_s^2}}$$

ii) **Miyamoto–Nagai disc:**

$$V_{\text{disc}}(x, y, z) = -\frac{GM_D}{\sqrt{x^2 + y^2 + (A + \sqrt{B^2 + z^2})^2}}$$

b) Bar component: $V_{\text{bar}}(x, y, z) = -\pi Gabc \frac{\rho_c}{n+1} \int_{\lambda}^{\infty} \frac{du}{\Delta(u)} (1 - m^2(u))^{n+1},$

(Ferrers bar)

$$\rho_c = \frac{105}{32\pi} \frac{GM_B}{abc}$$

$$\text{where } m^2(u) = \frac{x^2}{a^2 + u} + \frac{y^2}{b^2 + u} + \frac{z^2}{c^2 + u}, \Delta^2(u) = (a^2 + u)(b^2 + u)(c^2 + u),$$

n : positive integer ($n = 2$ for our model), λ : the unique positive solution of $m^2(\lambda) = 1$

Its density is:

$$\rho = \begin{cases} \rho_c (1 - m^2)^n, & \text{for } m \leq 1 \\ 0, & \text{for } m > 1 \end{cases}, \text{ where } m^2 = \frac{x^2}{a^2} + \frac{y^2}{b^2} + \frac{z^2}{c^2}, a > b > c \text{ and } n = 2.$$

Time-dependent barred galaxy model

The 3D bar rotates around its short z -axis (x : long axis and y : intermediate). The Hamiltonian that describes the motion for this model is:

$$H = \frac{1}{2}(p_x^2 + p_y^2 + p_z^2) + V(x, y, z, t) - \Omega_b(xp_y - yp_x) \equiv \text{Energy}$$

This model consists of the superposition of potentials describing an **axisymmetric** part and a **bar** component of the galaxy [Manos et al., J. Phys. A (2013)].

a) Axisymmetric component:

$$M_S + M_B(t) + M_D(t) = 1, \text{ with } M_B(t) = M_B(0) + \alpha t$$

i) **Plummer sphere:**

$$V_{\text{sphere}}(x, y, z) = -\frac{GM_S}{\sqrt{x^2 + y^2 + z^2 + \epsilon_s^2}}$$

ii) **Miyamoto–Nagai disc:**

$$V_{\text{disc}}(x, y, z) = -\frac{GM_D(t)}{\sqrt{x^2 + y^2 + (A + \sqrt{B^2 + z^2})^2}}$$

b) Bar component: $V_{\text{bar}}(x, y, z) = -\pi Gabc \frac{\rho_c}{n+1} \int_{\lambda}^{\infty} \frac{du}{\Delta(u)} (1 - m^2(u))^{n+1},$

(Ferrers bar)

$$\rho_c = \frac{105}{32\pi} \frac{GM_B(t)}{abc}$$

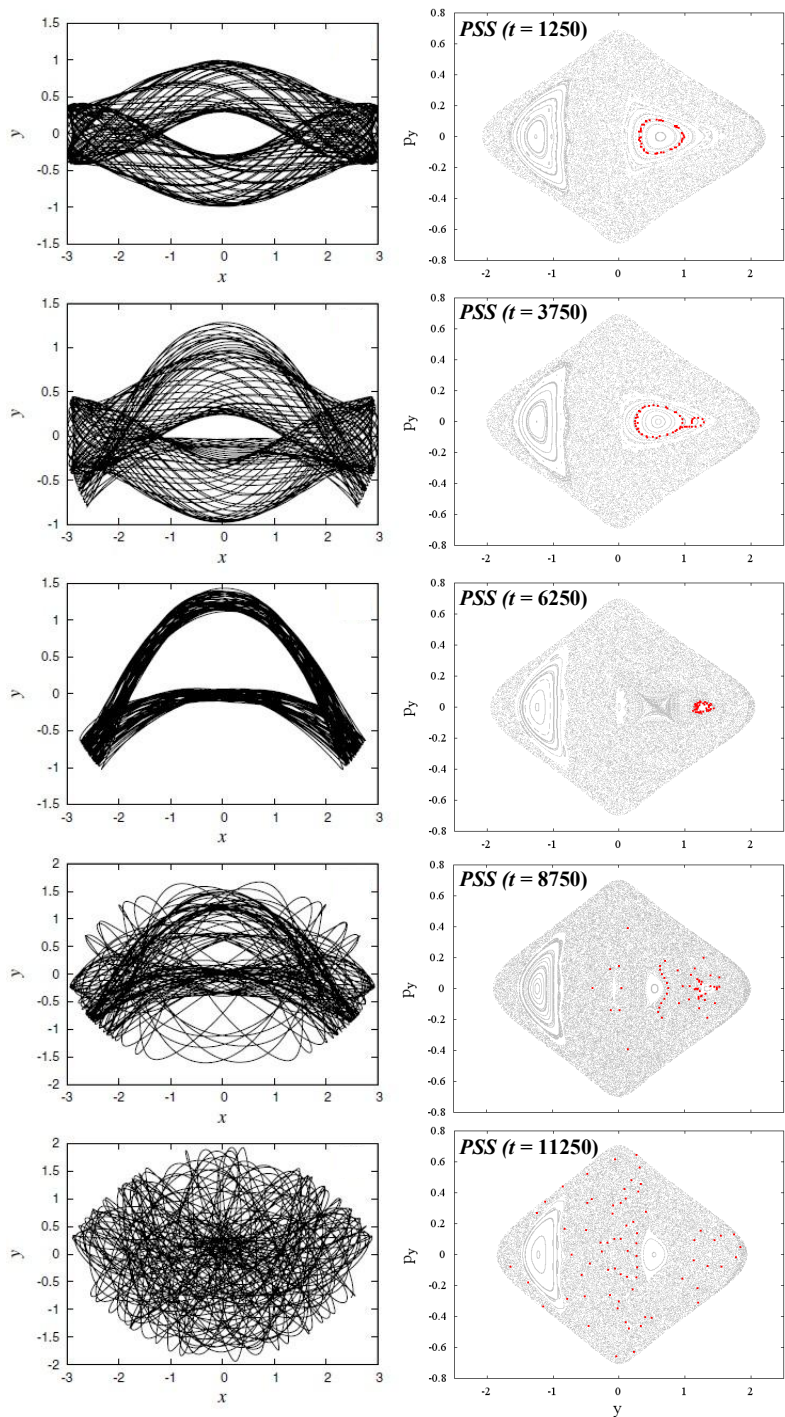
$$\text{where } m^2(u) = \frac{x^2}{a^2 + u} + \frac{y^2}{b^2 + u} + \frac{z^2}{c^2 + u}, \Delta^2(u) = (a^2 + u)(b^2 + u)(c^2 + u),$$

n : positive integer ($n = 2$ for our model), λ : the unique positive solution of $m^2(\lambda) = 1$

Its density is:

$$\rho = \begin{cases} \rho_c (1 - m^2)^n, & \text{for } m \leq 1 \\ 0, & \text{for } m > 1 \end{cases}, \text{ where } m^2 = \frac{x^2}{a^2} + \frac{y^2}{b^2} + \frac{z^2}{c^2}, a > b > c \text{ and } n = 2.$$

Time-dependent 2D barred galaxy model



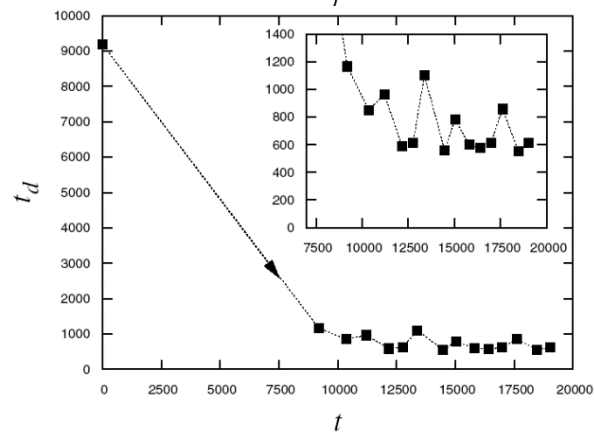
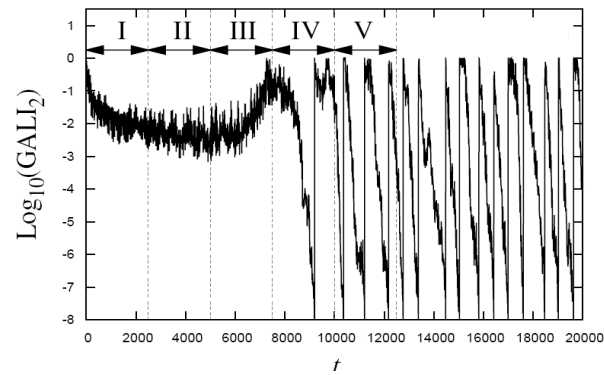
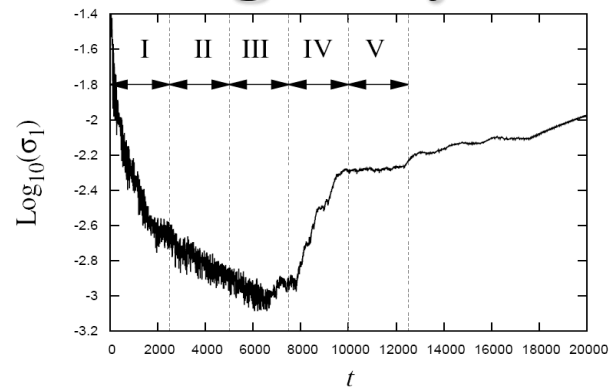
I

II

III

IV

V



A dissipative dynamical system

Lorenz system

We consider [Moges et al, IJBC (2025)] orbits leading to different dynamical behaviors for the 3D **Lorenz system** [Lorenz, J. Atmos. Sci. (1963)]:

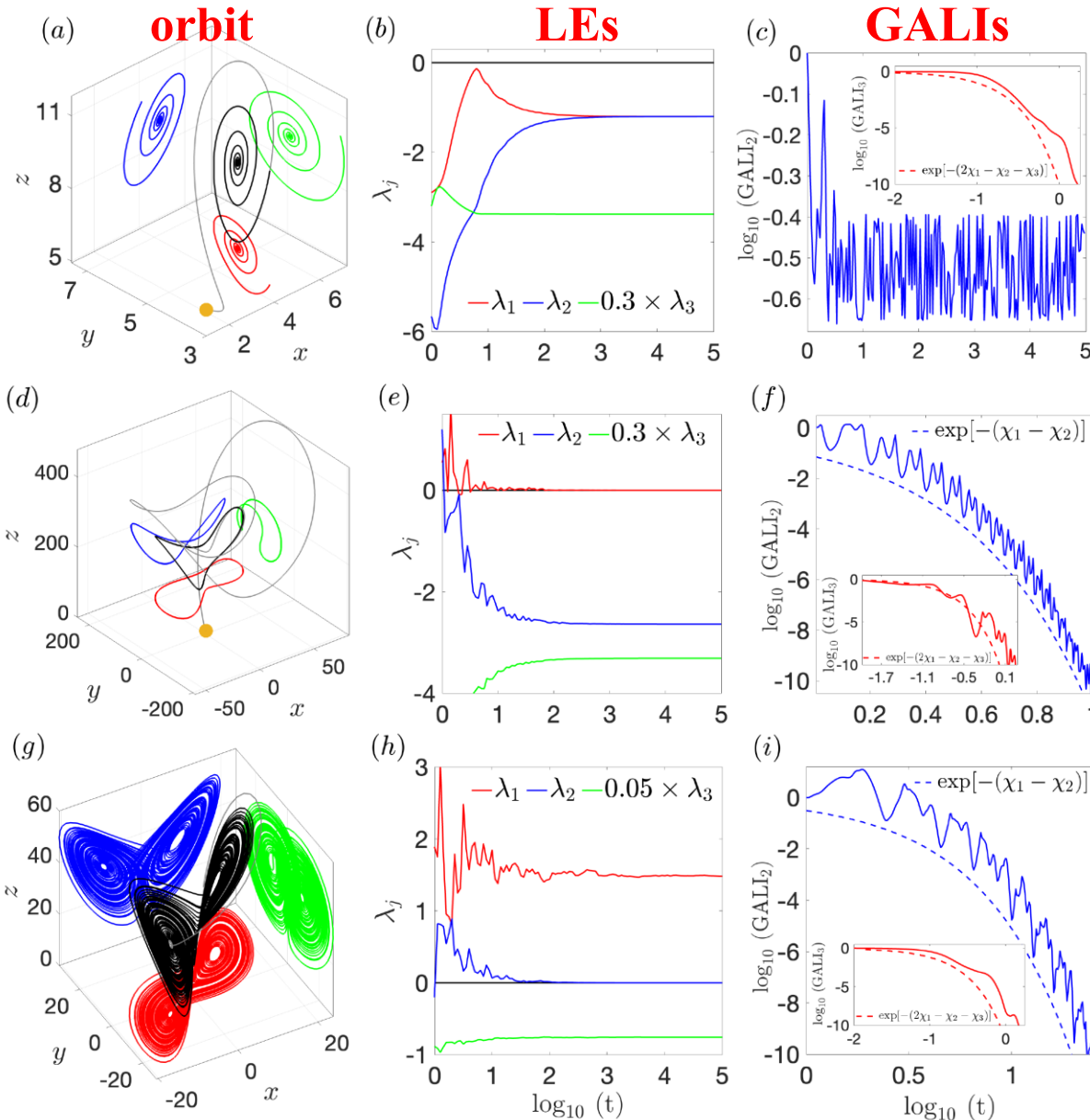
$$\begin{aligned}\frac{dx}{dt} &= a(y - x) \\ \frac{dy}{dt} &= rx - y - xz \\ \frac{dz}{dt} &= xy - bz\end{aligned}$$

In all cases GALI_k , $k=2, 3$, follows the evolution defined by:

$$\text{GALI}_k(t) \propto e^{-[(\lambda_1 - \lambda_2) + \dots + (\lambda_1 - \lambda_k)]t}$$

Lorenz system

We study the orbit with initial condition $(x, y, z) = (1, 3, 6)$ for $a = 10$, $b = 8/3$.



$r = 2.1$
stable fixed point

$r = 1.0$
stable limit cycle

$r = 33.3$
chaotic attractor

Chaos diagnostics based on Lagrangian descriptors (LDs)

Lagrangian descriptors (LDs)

The computation of LDs is based on the accumulation of some positive scalar value along the path of individual orbits.

Consider an N dimensional continuous time dynamical system

$$\dot{\mathbf{x}} = \frac{d\mathbf{x}(t)}{dt} = \mathbf{f}(\mathbf{x}, t)$$

The Arclength Definition [Madrid & Mancho, Chaos (2009) – Mendoza & Mancho, PRL (2010) – Mancho et al., Commun. Nonlin. Sci. Num. Simul. (2013)].

Forward time LD:

$$\text{LD}^f(\mathbf{x}, \tau) = \int_0^\tau \|\dot{\mathbf{x}}(t)\| dt$$

Backward time LD:

$$\text{LD}^b(\mathbf{x}, \tau) = \int_{-\tau}^0 \|\dot{\mathbf{x}}(t)\| dt$$

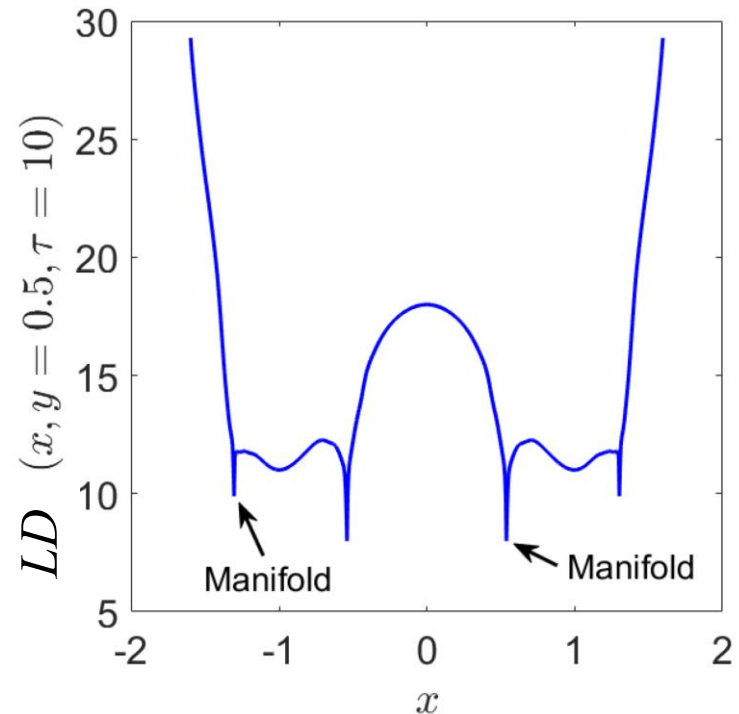
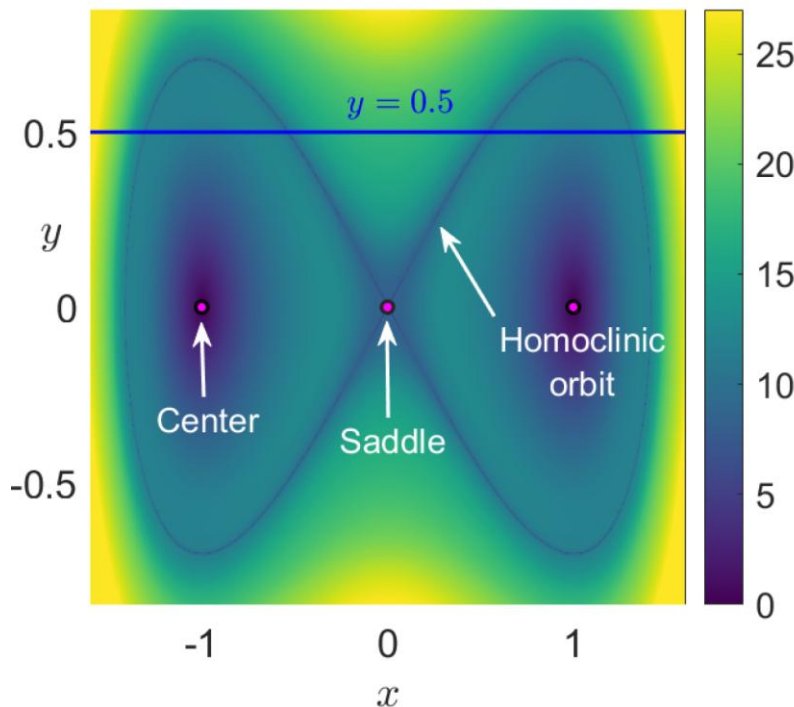
Combined LD:

$$\text{LD}(\mathbf{x}, \tau) = \text{LD}^b(\mathbf{x}, \tau) + \text{LD}^f(\mathbf{x}, \tau)$$

LDs: 1 dof Duffing Oscillator

$$H(x, y) = \frac{1}{2}y^2 + \frac{1}{4}x^4 - \frac{1}{2}x^2$$

The system has three equilibrium points: a saddle located at the origin and two diametrically opposed centers at the points $(\pm 1, 0)$.



From Agaoglou et al. 'Lagrangian descriptors: Discovery and quantification of phase space structure and transport', 2020, <https://doi.org/10.5281/zenodo.3958985>

The **location of the stable and unstable manifolds** can be extracted from the ridges of the **gradient field of the LDs** since they are located at points where the forward and the backward components of the LD are non-differentiable.

Lagrangian descriptors (LDs)

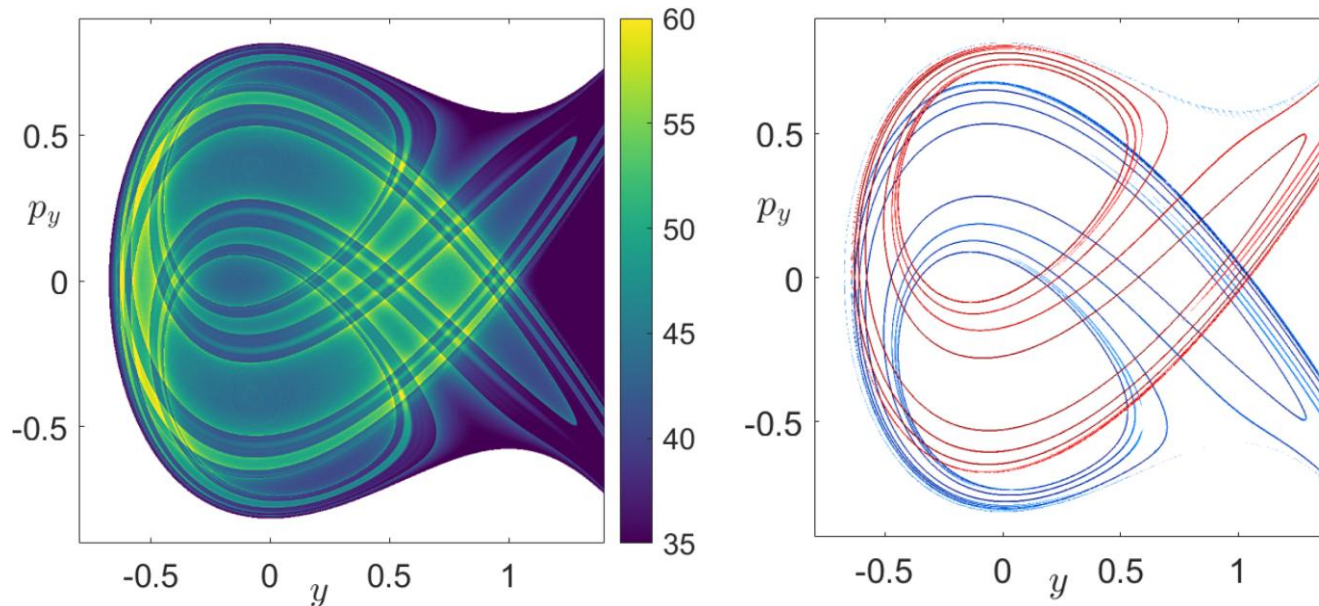
The ‘p-norm’ Definition [Lopesino et al., Commun. Nonlin. Sci. Num. Simul. (2015) – Lopesino et al., Int. J. Bifurc. Chaos (2017)].

Combined LD (usually $p=1/2$):

$$\text{LD}(\mathbf{x}, \tau) = \int_{-\tau}^{\tau} \left(\sum_{i=1}^N |\mathbf{f}_i(\mathbf{x}, t)|^p \right) dt$$

Hénon-Heiles system: $H = \frac{1}{2}(\mathbf{p}_x^2 + \mathbf{p}_y^2) + \frac{1}{2}(\mathbf{x}^2 + \mathbf{y}^2) + \mathbf{x}^2\mathbf{y} - \frac{1}{3}\mathbf{y}^3$

Stable and **unstable** manifolds for $H=1/3$, $\tau=10$.



Using LDs to quantify chaos

We consider orbits on a finite **grid of an $n(\geq 1)$ -dimensional subspace** of the **$N(\geq n)$ -dimensional phase space** of a dynamical system and their LDs.

Any non-boundary point \mathbf{x} in this subspace has **$2n$ nearest neighbors**

$$\mathbf{y}_i^\pm = \mathbf{x} \pm \sigma^{(i)} \mathbf{e}^{(i)}, \quad i = 1, 2, \dots, n,$$

where $\mathbf{e}^{(i)}$ is the i th usual basis vector in \mathbb{R}^n and $\sigma^{(i)}$ is the distance between successive grid points in this direction.

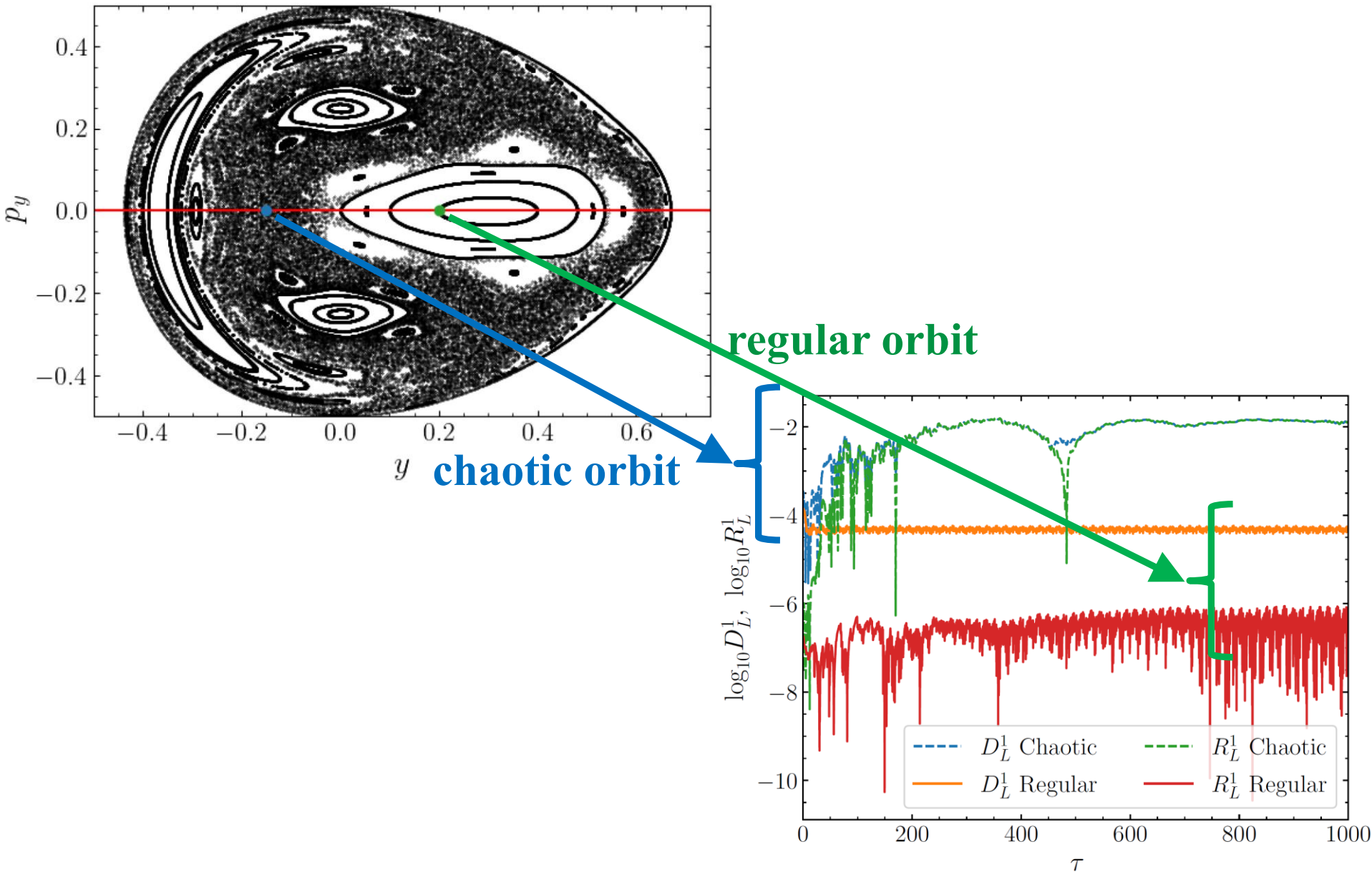
The **difference D_L^n** of neighboring orbits' LDs:

$$D_L^n(\mathbf{x}) = \frac{1}{2n} \sum_{i=1}^n \frac{|\text{LD}^f(\mathbf{x}) - \text{LD}^f(\mathbf{y}_i^+)| + |\text{LD}^f(\mathbf{x}) - \text{LD}^f(\mathbf{y}_i^-)|}{\text{LD}^f(\mathbf{x})}.$$

The **ratio R_L^n** of neighboring orbits' LDs:

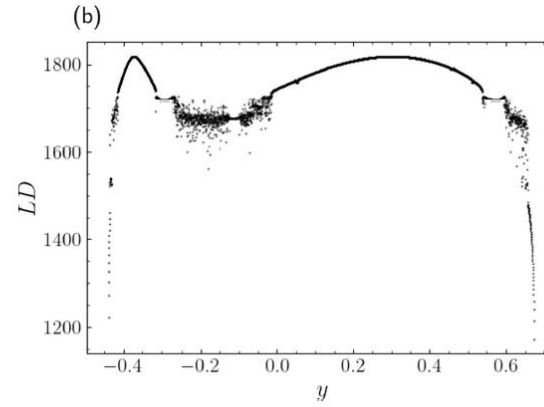
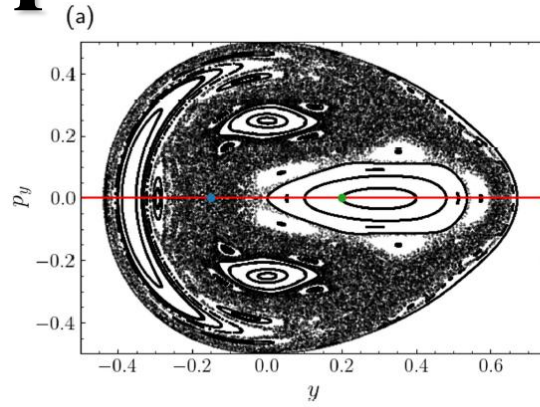
$$R_L^n(\mathbf{x}) = \left| 1 - \frac{1}{2n} \sum_{i=1}^n \frac{\text{LD}^f(\mathbf{y}_i^+) + \text{LD}^f(\mathbf{y}_i^-)}{\text{LD}^f(\mathbf{x})} \right|.$$

Application: Hénon-Heiles system



Application: Hénon-Heiles system

$H=1/8$

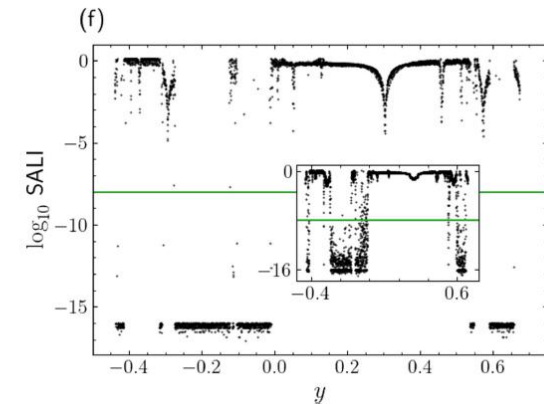
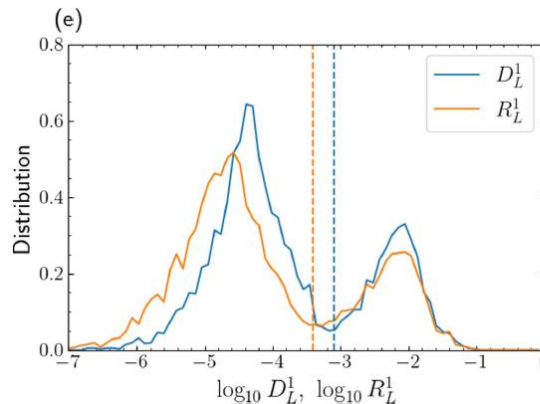
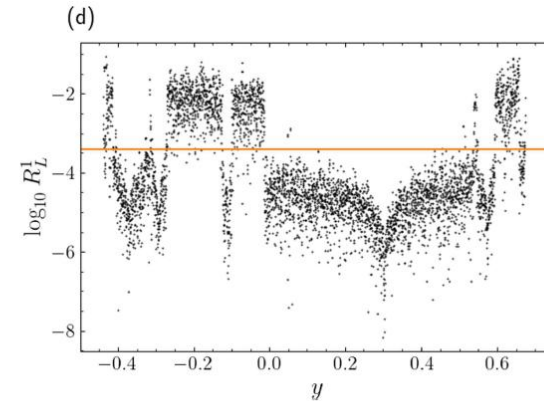
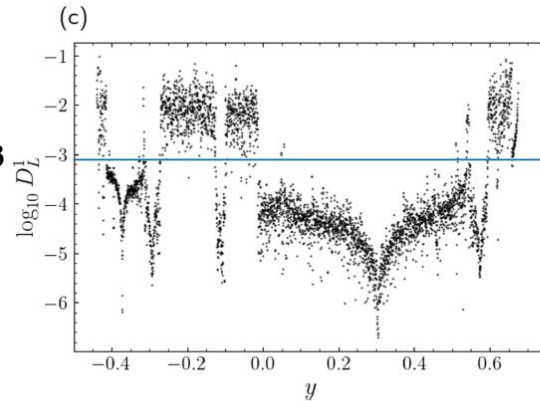


Variation of LDs with regard to initial conditions.

regular regions: smooth
chaotic regions: erratic

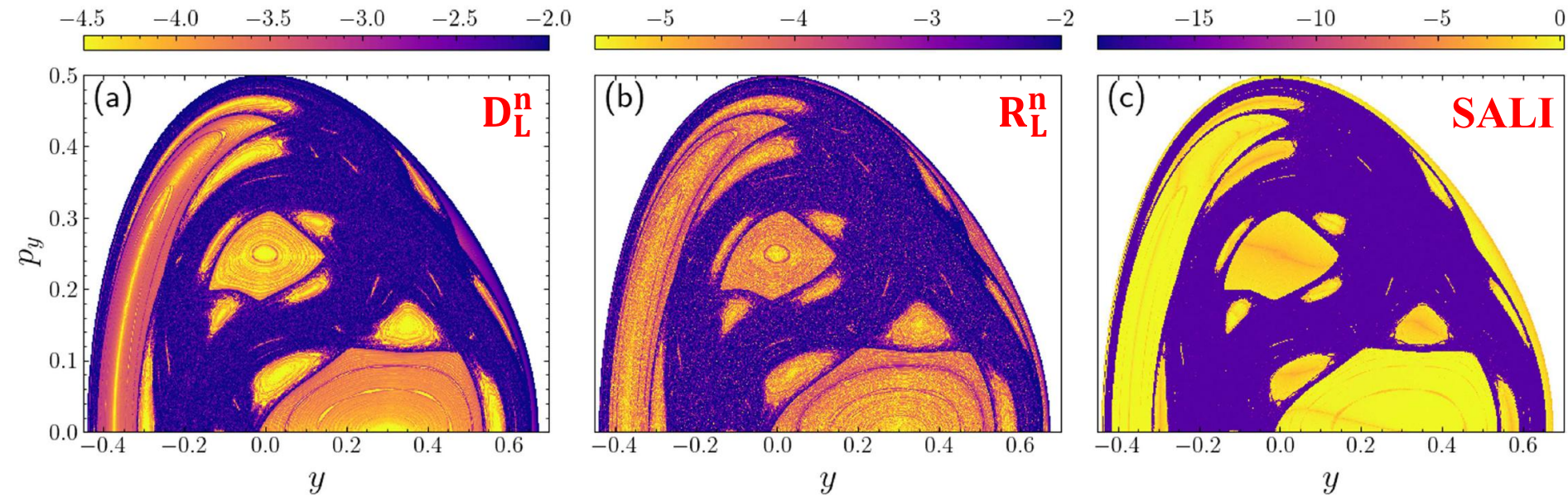
[also see Montes et al., Commun. Nonlin. Sci. Num. Simul. (2021)]

LDs for $\tau=10^3$

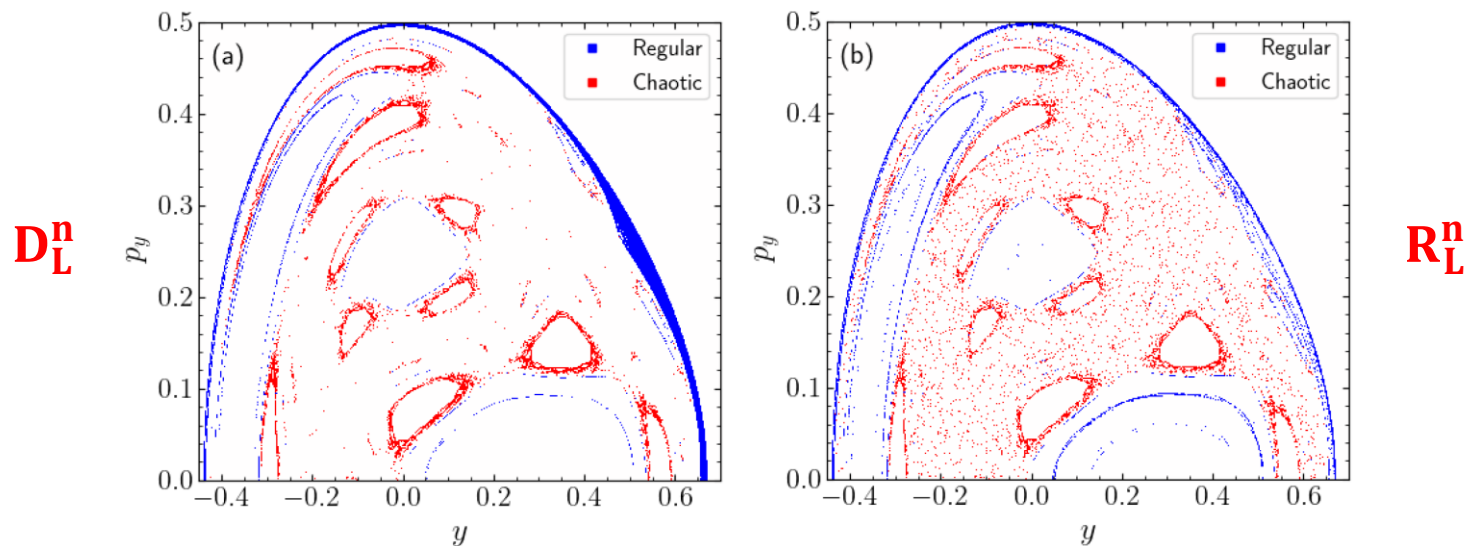


SALI for $\tau=10^6$
(inset $\tau=10^3$)

Application: Hénon-Heiles system



Misclassified orbits (< 10%)

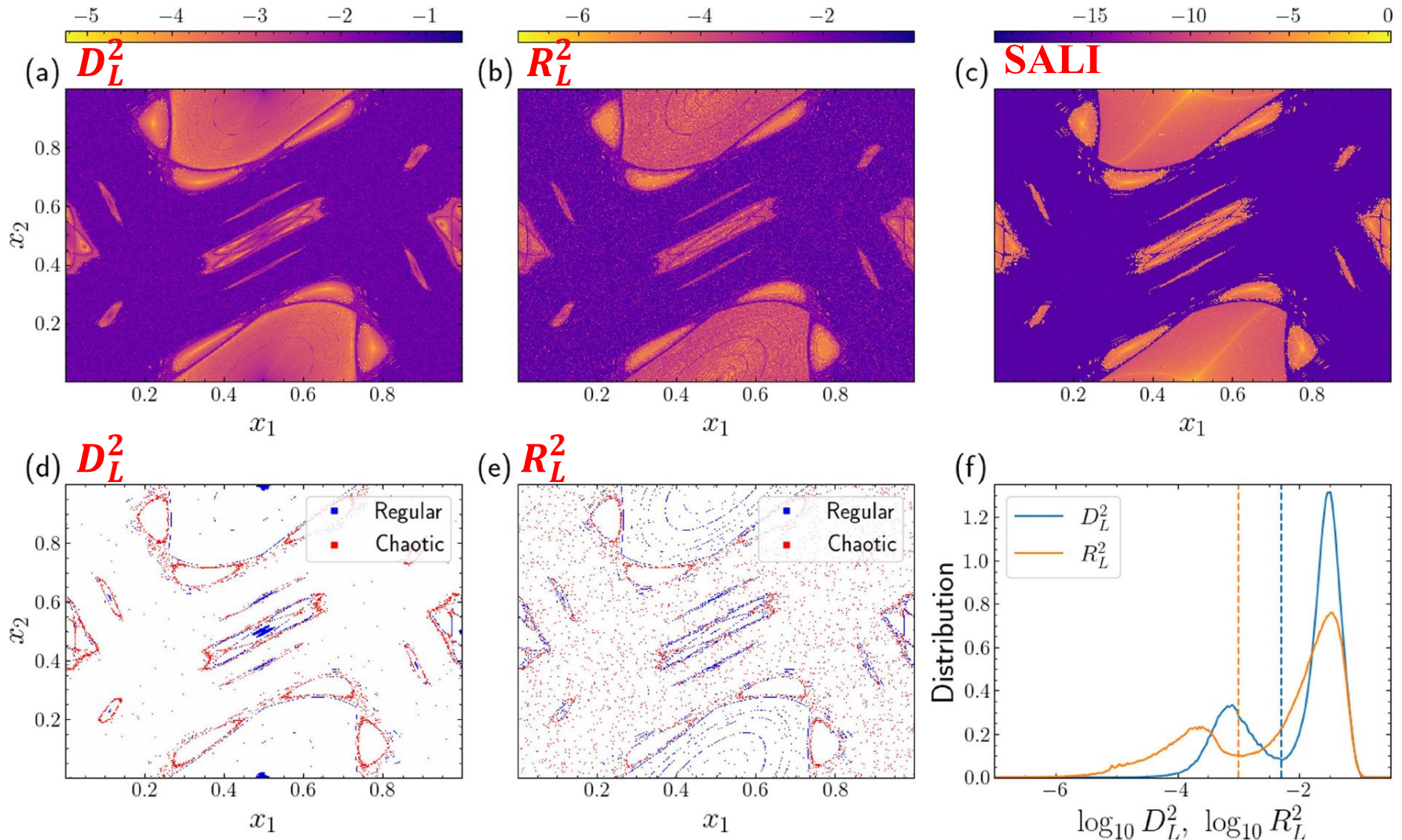


Application: 2D Standard map

We set $K = 1.5$

$$\begin{aligned} x'_1 &= x_1 + x'_2 \\ x'_2 &= x_2 + \frac{K}{2\pi} \sin(2\pi x_1) \pmod{1} \end{aligned}$$

Thresholds: $\log_{10} D_L^2 = -2.3$, $\log_{10} R_L^2 = -3$ ($T = 10^3$)
 $\log_{10} \text{SALI} = -12$ ($T = 10^5$)

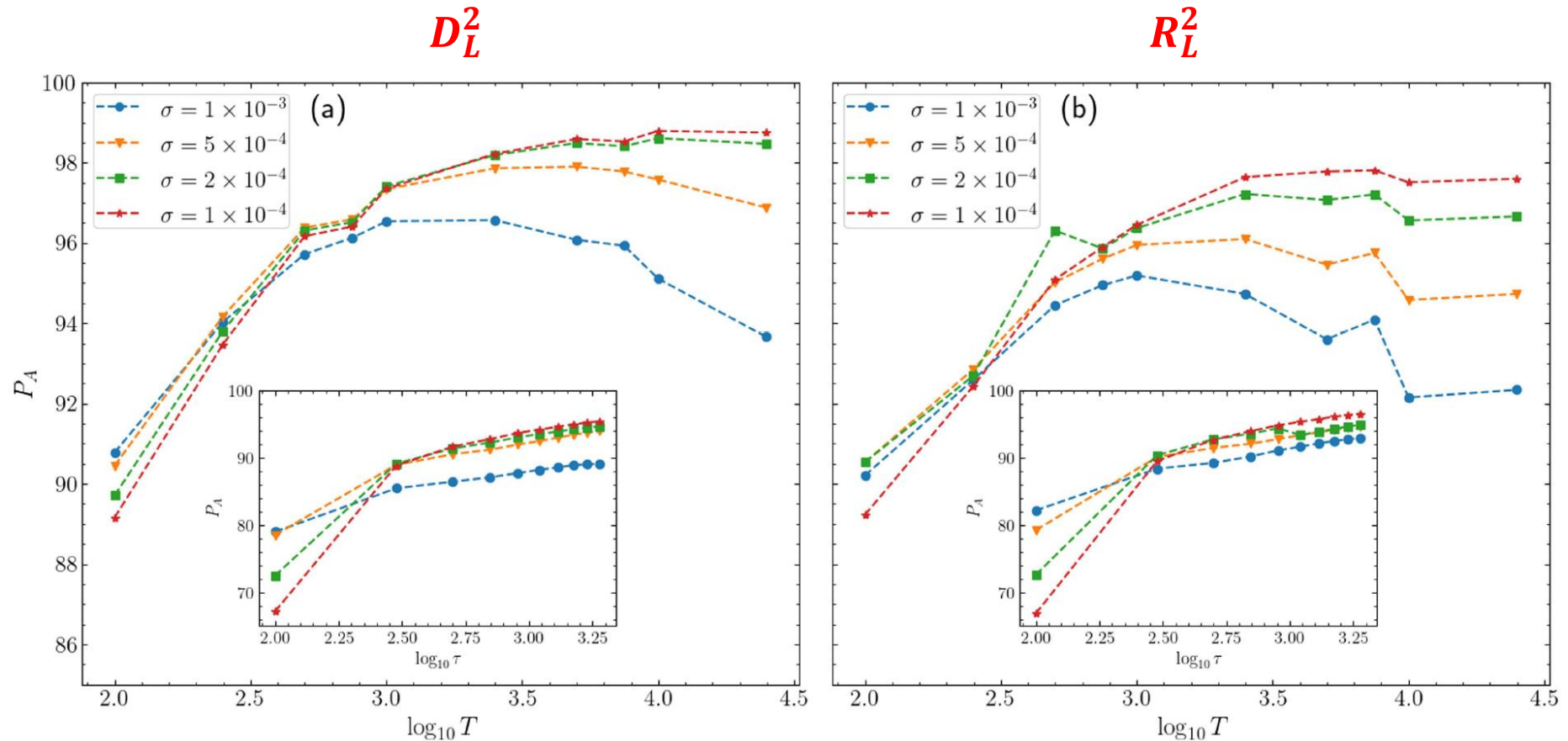


Effect of grid spacing (σ) and final integration time (T, τ)

P_A : percentage of correctly characterized orbits

Main plots: 2D Standard map

Insets: Hénon-Heiles system



Summary

- The Smaller (SALI) and the Generalized (GALI) ALignment Index methods are **fast, efficient and easy to compute chaos indicator**.
- Behaviour of the Generalized ALignment Index of order k ($GALI_k$):
 - ✓ **Chaotic motion: it tends exponentially to zero**
 - ✓ **Regular motion: it fluctuates around non-zero values (or goes to zero following power-laws)**
- $GALI_k$ indices :
 - ✓ **can distinguish rapidly and with certainty between regular and chaotic motion**
 - ✓ **can be used to characterize individual orbits as well as "chart" chaotic and regular domains in phase space**
 - ✓ **can identify regular motion on low-dimensional tori**
 - ✓ **are perfectly suited for studying the global dynamics of multidimensional systems, as well as of time-dependent models**
 - ✓ **they must be used with care in the case of dissipative systems**
- We introduced and successfully implemented computationally efficient ways to **effectively identify chaos in conservative dynamical systems from the values of LDs at neighboring initial conditions**.
 - ✓ **Advantages:**
 - **The indices show overall very good performance, as their classifications are in accordance with the ones obtained by the SALI at a level of at least 90% agreement.**
 - **Easy to compute (actually only the forward LDs are needed).**
 - **No need to know and to integrate the variational equations.**

Basic References

SALI

S. (2001) J. Phys. A, 34, 10029

S., Antonopoulos, Bountis & Vrahatis (2003) Prog. Theor. Phys. Supp., 150, 439

S., Antonopoulos, Bountis & Vrahatis (2004) J. Phys. A, 37, 6269

GALI

S., Bountis & Antonopoulos (2007) Physica D, 231, 30

S., Bountis & Antonopoulos (2008) Eur. Phys. J. Sp. Top., 165, 5

Manos, S. & Antonopoulos (2012) Int. J. Bifur. Chaos, 22, 1250218

Manos, Bountis & S. (2013) J. Phys. A, 46, 254017

Moges, Manos, Racoveany, S. (2025) Int. J. Bifur. Chaos, 35, 2530021

Reviews on SALI and GALI

Bountis & S. (2012) ‘Complex Hamiltonian Dynamics’, Chapter 5, Springer Series in Synergetics

S. & Manos (2016) Lect. Notes Phys., 915, 129

Lagrangian descriptors (LDs)

Madrid & Mancho (2009) Chaos, 19, 013111

Mendoza & Mancho (2010) Phys. Rev. Lett., 105, 038501

Mancho, Wiggins, Curbelo & Mendoza (2013) Com. Nonlin. Sci. Num. Simul., 18, 3530

Montes, Revuelta & Borondo (2021) Com. Nonlin. Sci. Num. Simul., 102, 105860

Daquin, Pédenon-Orlanducci, Agaoglou, García-Sánchez & Mancho (2022) Physica D, 442, 133520

Chaos diagnostics based on LDs

Hillebrand, Zimper, Ngapasare, Katsanikas, Wiggins & S. (2022) Chaos, 32, 123122

Zimper, Ngapasare, Hillebrand, Katsanikas, Wiggins & S. (2023) Physica D, 453, 133833

A ...shameless promotion

Contents

1. Parlitz: Estimating Lyapunov Exponents from Time Series
2. Lega, Guzzo, Froeschlé: Theory and Applications of the Fast Lyapunov Indicator (FLI) Method
3. Barrio: Theory and Applications of the Orthogonal Fast Lyapunov Indicator (OFLI and OFLI2) Methods
4. Cincotta, Giordano: Theory and Applications of the Mean Exponential Growth Factor of Nearby Orbits (MEGNO) Method
5. S., Manos: The Smaller (SALI) and the Generalized (GALI) Alignment Indices: Efficient Methods of Chaos Detection
6. Sándor, Maffione: The Relative Lyapunov Indicators: Theory and Application to Dynamical Astronomy
7. Gottwald, Melbourne: The 0-1 Test for Chaos: A Review
8. Siegert, Kantz: Prediction of Complex Dynamics: Who Cares About Chaos?

Lecture Notes in Physics 915

Charalampos (Haris) Skokos
Georg A. Gottwald
Jacques Laskar *Editors*

Chaos Detection and Predictability

 Springer

International Workshop, 2-6 February 2026

Cape Town, South Africa



WILHELM UND ELSE
HERAEUS-STIFTUNG



South African-German WE-Heraeus Seminar:
Nonlinear dynamics and anomalous transport

International Workshop 2 - 6 February 2026 Cape Town, South Africa

The study of unconventional dynamics and transport in low dimension has a long and distinguished history. It is thus perhaps surprising how much progress this field has seen in recent years, both in theory and experiment. This event is devoted to covering these developments in depth, starting from an introduction to the basics of the field and leading up to the cutting edge of current day research. The goal of this event is to bring together different communities which have studied anomalous dynamics and transport in low dimensions.

The format is chosen to maximise accessibility to a diverse set of participants. It is particularly aimed at researchers in the south of Africa, with an emphasis of career stages up to junior faculty. We aim to enable contacts between researchers based in Africa and in Germany at similar career stages, in the hope that these will persist as the researchers move ahead in their careers.

Topics include:

- Anomalous dynamics and transport
- Many-body dynamics
- Nonlinear and chaotic dynamics
- Nonlinear lattices
- Quantum transport
- Thermalization
- Non-Hermitian dynamics
- Large deviations
- Disordered systems



List of invited participants

Vassos Achilleos (FR)
Monika Aidelsburger* (DE)
Nora Alexeeva (SA)
Igor Barashenkov (SA)
André Botha (SA)
Pieter Claes (DE)
Fabian Essler (UK)
Florie Kunst (DE)
Stefano Lepri (IT)
Joel Moore (US)
Silvia Pappalardi (DE)
Tomas Prosen (SI)
Georgios Theodoridis (FR)
Hugo Touchette (SA)
Ruben Verresen (US)
Paul Woelfel (CM)
* to be confirmed

Scientific coordinators

Roderich Moessner
(MPI-PS Dresden)

Henri Skokos
(University of Cape Town)

Organisation
Kristina Alabiev
(MPI-PS Dresden)

Yvonne Brown
(University of Cape Town)

Applications received before 30 September 2025 are considered preferentially.

Applications are welcome and should be made by using the application form on the website of the event. Applications received before 30 September 2025 are considered preferentially. The number of attendees is limited.

For further information please contact:
heraeus26@pks.mpg.de
<https://www.pks.mpg.de/heraeus26>

Venue:
University of Cape Town
Graduate School of Business Conference Centre
Cape Town, South Africa

Topics include:

- Anomalous dynamics and transport
- Many-body dynamics
- Nonlinear and chaotic dynamics
- Nonlinear lattices
- Quantum transport
- Thermalization
- Non-Hermitian dynamics
- Large deviations
- Disordered systems

The event is particularly aimed at researchers of career stages up to junior faculty.

The number of participants is limited to around 50 people.

Webpage:

<https://www.pks.mpg.de/heraeus26>

